University of Zurich, Physics department

Coherent quantum transport in anisotropic two dimensional systems in magnetic fields

Simon Flury

Master thesis

supervised by
Dr. Mark Fischer
Prof.Dr. Titus Neupert

May, 2020

Abstract

The transport of electrons in the bulk of a metal is usually well captured by their particle-like aspects, while their wave-like nature is commonly harder to observe. This is the case, because the phase information in the bulk is lost, due to the high electron density and interaction with the ionic background. However, in mesoscopic systems the quantum phase reveals. Recent observations of a new type of phase coherent oscillation, in the out-of-plane magnetoresistance of quasi two dimensional anisotropic systems, has shown a remarkable phase coherence over several length scales. The following work includes a detailed study of the effect of anisotropy on a two dimensional mesoscopic system, under the influence of a homogeneous magnetic field. We observed a reduced effect of the magnetic field on the electronic spectrum in the vicinity of strong anisotropy. Depending on the in-plane dimension, anisotropy affects with a different strength. Calculating electronic conductivity, using the two well elaborated approaches by Kubo and Landauer, will show the influence of different anisotropy on coherent quantum transport. Whereas the Landauer formula is simpler in handling, the Kubo formula will give the chance to approximate systems at much higher width, due to a separate evaluation of intra- and inter-band contributions.

Contents

1. Introduction

In vacuum electrons carry the characteristics of particles as well as waves. This was demonstrated the interference experiments of Davisson and Germer (1928) [1]. Due to the high electron density and interaction with the ionic lattice, the phase information is lost in bulk phenomena. Thus transport of electrons in metals is usually well described by the semi-classical Boltzmann equation, using only the particle nature of the electrons. However, in systems of mesoscopic length scale, the phase of the electron is preserved an becoming observable in electronic transport. One of the most famous example of it is the Aharonov-Bohm effect (ABE) in nanoscopic rings of gold [2]. There, the effect of the vector potential is leading to an oscillation, periodic in the magnetic field B (see Appendix A). Due to huge experimental progress, the construction of mesoscopic quasi two dimensional layered structures, with highly conducting metallic layers were possible, such that the phase information is preserved [3].

In general the period, of all field-induced oscillations in quantum objects, is given by an integer multiple of the flux quantum threading through them, $B_n \cdot S = n\phi_0$. In metallic systems, the relevant length scales is usually given by the cyclotron radius r_c, leading to an oscillation periodic in $1/B$ ($B_n \cdot r_c^2 \propto n\phi_0$). A well known of such a $1/B$ periodic oscillation is given by the Shubnikov-de-Haas effect (SdH) [4]. These oscillations are caused by the variation of the number of electrons at the Fermi surface. The magnetic field arrange the states in discrete Landau levels, broadened by disorder and finite temperature, associated with a large density of states (DOS). An increase of the magnetic field pushes the levels across the Fermi level Fig.1, leading to an oscillation in the DOS at the Fermi level. This picture breaks down, if the orbits are open and the cyclotron radius diverge. In such a case SdH-oscillations will not appear. In layered structures, this is the case if the magnetic field is turned completely in-plane, where no oscillations are expected.

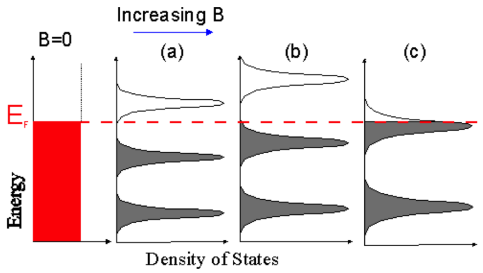

Figure 1: Schematics of the Landau level behaviour under the influence of an increasing field. The x-axis shows the DOS and the y-axis the energy. Picture a,b,c give the position in energy of the highest filled Landau level in the vicinity of the Fermi energy, for increasing B-field.

Recent experimental studies on the quasi two dimensional layered structure of ultra pure delafossites, for the case of an in-plane magnetic field, revealed a new type of

phase coherent oscillation in the out-of-plane magnetoresistance. [5]. Those systems consist of highly conducting layers separated by insulating ones, resulting in a large transport anisotropy. The reported oscillations has an oscillation period equivalent to that determined by the magnetic flux quantum h/e, threading an area defined by the atomic interlayer separation and the sample width, thus a B-periodic oscillation Fig.2. The phase shows a remarkable robustness over macroscopic length scales exceeding $10\mu m$ and temperatures up to $50K$, that contradicts a description akin to ABE (see Appendix A).

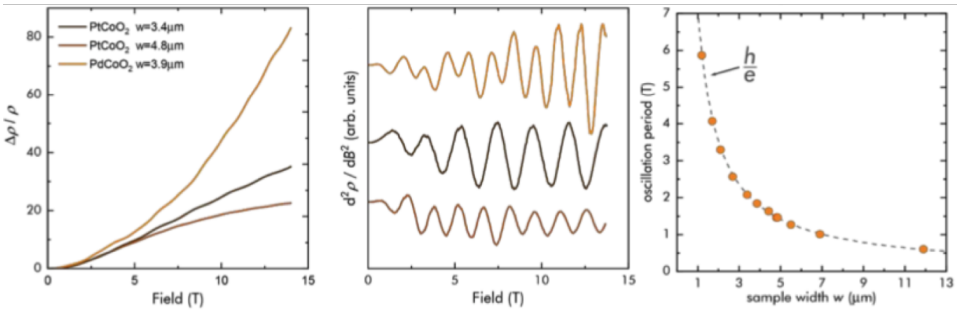

Figure 2: Experimentally observed results for the magnetoresistance of the out-of-plane transport [5]. **Left**: Magnetoresistance at $T = 2K$ for various sample widths. At high fields a difference in background appears due to the influence of angle dependent magnetoresistance. **Middle**: Second derivative of the resistivity shows the oscillatory behaviour of the magnetoresistance. **Right**: Oscillation period as function of sample width, in agreement with a magnetic flux of h/e pierces the area spanned by the sample with and the atomic interlayer separation.

These observations and the possibility to build system of the required dimensions support the study of coherent quantum transport in anisotropic two dimensional systems in magnetic fields. The reduced dimension in one direction turns the energy spectrum from a continuous one to discrete levels. This introduces the level spacing as a parameter in the electronic model. The interplay between anisotropy, level spacing, temperature and magnetic field has different effects on the energy spectrum and on transport properties. The following work will show some of these effects and give an answer to the question which of them survive if the limit to large systems is taken.

Electronic transport in mesoscopic systems is usually well described by the Landauer formula which uses a scattering matrix approach. Because of electronic transport is in its nature a many-body behaviour, treating it with many-body theories like Kubo's quantum transport theory is useful. The approaches gives as similar result in the case of DC currents in the thermodynamic limit. The effect of using finite system lengths and anisotropy is at this date unknown. It is therefore questionable if the two approach will still lead to the same result.

In the following, three question are the building blocks of this work and will be answered in it.

-) How does anisotropy and finite level spacing affect the electronic spectrum and the quantum coherent transport, in a homogeneous magnetic field.

-) Which transport formula reveals the experimentally observed behaviour and under what circumstances they deliver a comparable result.

-) Does the effects of anisotropy survive in the limit of continuous energy spectrum or are they reduced to just a general scaling factor.

2. Mesoscopic Systems

The main characteristic of an electronic mesoscopic system is that the electron can keep its wavefunction phase-coherent throughout the sample. In a microscopic system the energy levels are discrete and so the physical properties are mainly controlled by quantum behavior. In macroscopical systems, classical and semiclassical descriptions can be used. For example, the conductivity in this case is determined by the average scattering rate. Thus the assumption of isotropic Boltzmann transport theory can be used. With increasing temperature, inelastic scattering by lattice vibrations occurs at high rate based on the fact that the inelastic scattering time τ_{in} satisfies $1/\tau_{in} \approx k_B T/\hbar \approx 10^{13}\mathrm{s}^{-1}$, so $\tau_{in} \simeq 10^{-13}$s. The inelastic scattering mean free path is give by $l_{in} = v_F \tau_{in} \approx 1000\mathring{A}$, where $v_F \approx 10^{16}\mathring{A}/s$ is the Fermi velocity. Therefore in macroscopic sample at room temperature the phase information is always destroyed. The typical length over which the phase remains coherent is the elastic mean free path which is about $100\mathring{A}$. In this case electrons can be treated as semiclassical particles. There the wave aspects are smeared out and only the local interference correction in the conductivity needs to be considered [6].

In the case of mesoscopic systems, at low temperature the coherence length of the wave will be larger than the sample size, then the Boltzmann approach is not appropriate. At this length scales quantum coherence will be important.

2.1. Transport regimes

For electron transport there are two kind of descriptions.

$$\vec{j} = \sigma \vec{E} \qquad \text{and} \qquad I = GV. \tag{1}$$

The first is a local one, where the conductivity σ relates the local current density $\vec{j}$ to the electric field $\vec{E}$. The second is a global one in which the relation between the total current I and the voltage drop V is given by the conductance G.

The relation between conductance and conductivity for a large homogeneous conductor is given by

$$G = \sigma L^{d-2}. \tag{2}$$

Even if in mesoscopic systems the measured quantities are the non-local ones, the behaviour can be studied from the conductance as well as from the conductivity, for the case of a homogeneous system. We will concentrate on the local quantities, to be able to compare with the experimental observed results in [5]. There are several characteristic length scales in mesoscopic structures, such as the system length L, width W, elastic mean free path l and the localization length ξ [6]. By this scales one can define three different regimes for electron transport in mesoscopic structures Fig.3.

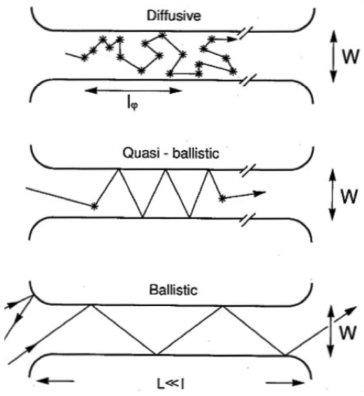

Figure 3: Electron trajectories for the diffusive (l < W, L), quasi-ballistic (W < l < L) and ballistic (l > W, L) transport regimes [6].

-) **Ballistic** (W,L < l < ξ): impurity scattering can be neglected and electron scattering occurs only at the boundaries.

-) **Quasi-ballistic** (W < l < L < ξ): boundary and internal impurity scatterings are of equal importance.

-) **Diffusive** (l < W,L < ξ) : the sample contain a significant amount of impurities or structural disorder, leading to $l \sim 100\mathring{A}$ the elastic scattering length, independent of temperature. In this the physical picture of electron transport is given by a random walk.

Mean free path l
The mean free path describes the average length between two scattering events. It is described by

$$l = \nu_F \tau_{scat}, \tag{3}$$

with ν_F the Fermi velocity and τ_{scat} the average scattering time.

Beside this variables, adding a magnetic field and finite temperature, two other lengths scales are relevant.

Thermal length L_T
At finite temperatures only electrons in a range of a few $k_B T$ around the Fermi energy E_F contribute to the transport. The thermal length is the length an electron travels, started at E_F with its momentum in a certain directions, until it differs one radian in phase compared to an electron at an energy $E_F + k_B T$.

$$L_T = \frac{\hbar \nu_F}{k_B T} \tag{4}$$

Magnetic length l_B

An important quantity, when adding a magnetic field, is the area $A = \hbar/eB$ threaded by one magnetic flux quantum. Thus the corresponding length scale is given by

$$l_B = \sqrt{\hbar/eB} \tag{5}$$

2.2. Phase coherent transport

Speaking about phase coherent transport two quantities are of main interest. The coherence time τ_ϕ and the coherence length ξ_ϕ. They are related in the case of ballistic samples by the Fermi velocity [7]

$$\xi_\phi = v_F \tau_\phi. \tag{6}$$

It is well known that in quantum mechanics electrons carry a phase. If waves interfere, the phase difference $\Delta\phi$ becomes relevant. Holding this difference constant is known as phase coherence. The coherence time is defined as the average time, by which any such interference term for a specific time t is suppressed by $\exp(-t/\tau_\phi)$. One could think that scattering at impurities or defects changing phase, but this is in fact not the case. Scattering at rigid scatterers can add an additional phase to the particle that is static, such that it just shifts the interference pattern. Dynamic or fluctuating scatterers however, lead to a time dependent phase $\phi(t)$, for which the time average is zero if $t \gg \tau_\phi$

$$\langle\phi\rangle_t = \int_0^t \phi(t')dt' \sim 0, \tag{7}$$

such that the interference term

$$\langle\exp(i\phi(t'))\rangle_t \sim \exp(-t/\tau_\phi) \tag{8}$$

is exponentially suppressed due to the loss of phase coherence. Thus the time-averaged interference turns to zero because of phase coherence. Due to eq.(6), ξ_ϕ is the length scale over which the phase remains coherent. If the system dimension is less than the coherence length, the system is said to be in the coherent transport regime. To reach this regime the sources of decoherence have to be neglectable, like electron-electron scattering or electron-phonon scattering. Later is the case for low temperatures. If also impurity scattering is absent or highly suppressed, the resulting transport is in the ballistic regime.

In the mesoscopic regime the electron dynamics is described by a quantum description (Schroedinger equation), but the coherent dynamics is interrupted due to scattering processes. Therefore this regime has to be treated with many-body-techniques like the linear response theory by Kubo. In our work we will neglect electron-electron scattering and include electron-phonon scattering just as an impact to the life time. Thus the phases between different sites remains coherent leading to coherent transport.

2.3. Weak localization

Weak localization is an effect of scattering on weak disorder. Weak disorder means that the mean free path l is much greater than the characteristic wavelength λ and less then the size of the sample L. Because of the wave-like character of particles, it is more instructive to study the wave behaviour for the propagation of classical waves in disordered media. We look at the path of a wave diffusing from the origin O to some point O'. The transport between this two points can take place along different trajectories, with probability amplitude A_i connected to every path i. The total intensity I to reach O' from O is given by

$$I = \left| \sum_i A_i \right|^2 = \sum_i |A_i|^2 + \sum_{i \neq j} A_i A_j^*, \tag{9}$$

where the second term describes the interference of the paths. In most cases, this term is not important and can be neglected, because the trajectories have different lengths and amplitudes A_i, carry different phases. One average this leads to destructive interference. This argumentation is not valid in the case where $O = O'$ i.e. if the path crosses itself. The path can be traversed in two opposite directions (forward and backward), and the probability of one direction is the return probability of the other. Since the two paths are identical, the amplitudes A_1, A_2 are phase coherent. This leads to constructive interference, so that the wave contribution to the probability $p(\vec{r}, t)$, of the particle being at position $\vec{r}$ at time t, becomes very important and eq.(9) tells us that for $A_1 = A_2 = A$, the classical return probability is given by $2|A|^2$, while the wave character yields $2|A|^2 + 2A_1 A_2^* = 4|A|^2$. Thus the probability for a wave to return to the starting points is twice that of a classical particle. This means weaves in a disordered medium are less mobile than classical particles.

2.4. Structure details

The structures we are going to study are given by two dimensional lattices, which are of finite dimension in x-direction and infinite dimension in y-direction. This can be reached by applying periodic boundary conditions in y-direction, then the underlying lattice Hamiltonian can be diagonalized (see section 3.1) or by attaching leads (see section 4.1). By varying the hopping anisotropy and the width, different transport regimens can be modelled. A low width and strong hopping in x-direction simulate the ballistic transport regime in which we will work in the following. Adding small amount of impurities can show the effect of weak localization.

Such two dimensional lattices are ideal to model quasi two dimensional systems like the layered structure of ultra-pure delafossites studied in [5]. Those systems are in-plane of mesoscopic dimension and out-of-plane of macroscopic dimension. The conducting layers consist of the ultra-pure metals Pt/Pd, separated by isolating layers of CoO_2, reflected in a large anisotropy of $\rho_y/\rho_x \sim 1000$ and a mean free path larger than the lattice width. Fig.4 shows the modelling of the delafossites by a square lattice.

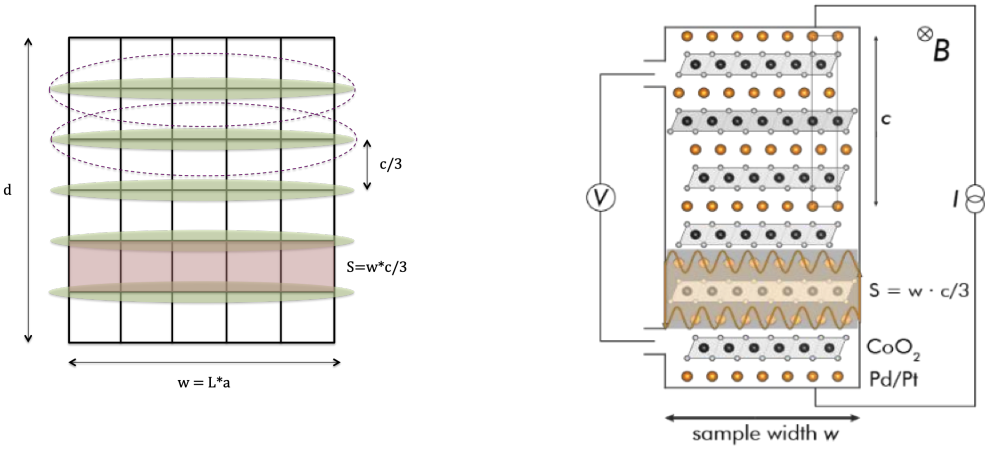

Figure 4: **Left:** Schematic of a 2-dim. square lattice, that corresponds to the system given on the right. In green the extended standing waves states are drawn. Shrinking the distance between adjacent layers lead to an overlap of the wave functions (violet ellipses) and non-vanishing tunnel probability **Right:** Graphical illustration of the experimentally analysed system and its layered structure. The colored area S, in both graphics, correspond to the one pierced by one flux quantum [5]

.

The area, that pierced by one magnetic flux quantum $\phi_0 = h/e$ matches the period of the oscillation in the magnetoresistance, is given by $S = w \cdot c/3$. There w is the width of the system and c the cristallographic unit cell. Due to the ABC-stacking of the structure, the distance between two adjacent layers is given by $c/3$. In the lattice the area is given

be the lattice width $L \cdot a$ and the lattice constant a. In terms of the in eq.(5) introduced length scale, a condition on the width can be derived

$$w = 3 \cdot l_b^2 \cdot c. \tag{10}$$

Due to the large anisotropy the states near the Fermi energy are in a standing wave state extended over the layer, shown as green clouds in the left plot of Fig.4. Thus contains full phase coherence over the entire sample width. For a large distance in y-direction, no transport would be possible. Because of the small inter-layer distance in the delafossites the wave functions overlap, what results in a finite electron transport. The overlap of the wave functions due to decreasing layer distance is sketched as violet ellipses in Fig.4.

To be able to compare the results of our transport calculations, using Landauer or Kubo approach, with the experimentally observed oscillations, the specific sample informations are needed. Those are extracted from [5] and summarized in table 1.

Sample information

w(μm)	c(nm)	d(μm)	l(μm)	$\xi_\phi(nm)$
$1.2 - 12$	(Pd)1.775, (Pt)1.781	$9 - 22.3$	~ 20	~ 400

Table 1: Sample information taken from [5]. (w) sample width, (c) crystllographic unit cell, (d) sample length, (l) mean free path, (ξ_ϕ) coherence length. The mean free path was obtained from a Dingle analysis and the coherence length extracted from SdH oscillations.

3. Effect of Magnetic Field on a Lattice Model

To study the effect of a magnetic field on a lattice model, we consider a square lattice with lattice constant a and hopping amplitude t. The position on the lattice is defined by $\vec{x} = a(m, n)$ where $m, n \in \mathbb{Z}$. The Hamiltonian in real space representation takes the form

$$H = -t \sum_{\vec{x}} \sum_{j=1,2} |\vec{x}\rangle\langle\vec{x} + \vec{e}_j| + h.c. \tag{11}$$

with $\vec{e}_1 = (a, 0)$ and $\vec{e}_2 = (0, a)$. Because of the translational invariance of the Hamiltonian, states can be labeled by their momenta as quantum numbers. This is based on the fact that the Hamiltonian commutes with the translation operator. The momenta are given by $-\frac{\pi}{a} < k_x, k_y \leq \frac{\pi}{a}$ and define a torus $\mathcal{T}^2$ called Brillouin zone (BZ). For a lattice of size $L_x \times L_y$ the momenta are quantised in units of $\frac{1}{2\pi L_j}$. Then, the number of states in the BZ is given by $\left(\frac{2\pi}{a} / \frac{1}{2\pi L_x}\right) \times \left(\frac{2\pi}{a} / \frac{1}{2\pi L_y}\right) = L_x L_y / a^2$, which is equivalent to the number of sites in the lattice and so the number of states in the Hilbert space.

Adding a magnetic field to the Hamiltonian defined in eq.(11), is done by the Peierls substitution named after his inventor Rudolf Peierls.

$$H = -t \sum_{\vec{x}} \sum_{j=1,2} e^{-iea A_j(\vec{x})/\hbar} |\vec{x}\rangle\langle\vec{x} + \vec{e}_j| + h.c. \tag{12}$$

This has the effect, that a particle moving around a plaquette picks up a phase factor $e^{-i\gamma}$ Fig.(5).

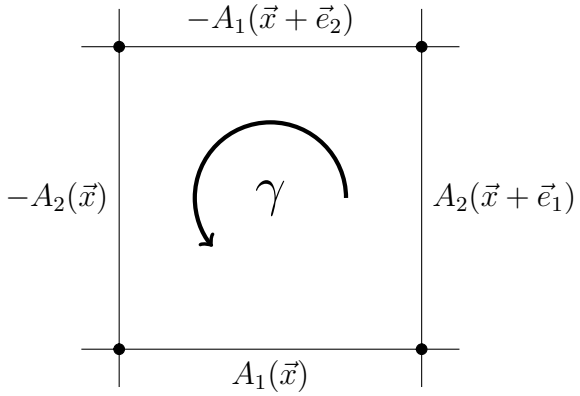

Figure 5: Schmatic drawing of one plaquette of the lattice. Going counter clockwise around the plaquette a phase of γ is picked up.

The phase γ is given by

$$\begin{aligned} \gamma &= \frac{ea}{\hbar} \left(A_1(\vec{x}) + A_2(\vec{x} + \vec{e}_1) - A_1(\vec{x} + \vec{e}_2) - A_2(\vec{x})\right) \\ &\approx \frac{ea^2}{\hbar} \left(\frac{\partial A_2}{\partial x_1} - \frac{\partial A_1}{\partial x_2}\right) = \frac{ea^2 B}{\hbar}, \end{aligned} \tag{13}$$

which is equivalent to a Aharonov-Bohm phase $\Phi_{AB} = Ba^2$. For the following, we will work in Landau gauge $A_1 = 0$, $A_2 = Bx_1$. A question that arises is whether the BZ changes or even exist in the presence of the magnetic field. The existence of momenta $\vec{k}$ is a consequence of translational invariance of the lattice, but the choice of gauge breaks this invariance explicitly. As a solution one can define the magnetic BZ. This is possible if $\Phi = 2\pi\frac{p}{q}$, with $p, q \in \mathbb{Z}$ and share no common divisor. Φ is written in units of ϕ_0. Then, the spectrum splits up into q different bands, whereas if $\frac{p}{q}$ is irrational there are no distinct bands and the spectrum takes the form of a cantor set. We will come back to this situation in the next section.

To show this explicitly, we can write the Hamiltonian in terms of the gauge invariant translation operators $\hat{T}_j = \sum_{\vec{x}} e^{-iea A_j(\vec{x})/\hbar} |\vec{x}\rangle\langle\vec{x} + \vec{e}_j|$

$$\hat{H} = -t \sum_{j=1,2} \left(\hat{T}_j + \hat{T}_j^\dagger\right). \tag{14}$$

The translation operators do not commute

$$\hat{T}_2\hat{T}_1 = e^{i\Phi}\hat{T}_1\hat{T}_2 \rightarrow [\hat{T}_i, \hat{T}_j] \neq 0, \tag{15}$$

what results in non commutation of the translation operators and the Hamiltonian, such that the momentum $\vec{k}$ is not a good quantum number and the states cannot be labeled with it. To find the new symmetries of the lattice Hamiltonian with flux and to recover translational invariance, new operators have to be constructed.

$$\hat{T}_j^M = \sum_{\vec{x}} e^{-iea A_j^M(\vec{x})/\hbar} |\vec{x}\rangle\langle\vec{x} + \vec{e}_j|, \tag{16}$$

where A_j^M is the new gauge field constructed by $\partial_k A_j^M = \partial_j A_k$. In Landau gauge this leads to $A_1^M = Bx_2$ and $A_2^M = 0$. Then the new operators commute with the Hamiltonian but not with themselves, thus one can label states by eigenvalues of $\hat{T}_1^M$ but not simultaneously by eigenvalues of $\hat{T}_2^M$.

$$\hat{T}_2^M\hat{T}_1^M = e^{i\Phi}\hat{T}_1^M\hat{T}_2^M. \tag{17}$$

As a consequence the commutator vanishes only if Φ is an integer multiple of 2π. Such a flux configuration is gauge-equivalent to the trivial case of zero flux per plaquette and therefore not to the situation we are interested in. For flux values different from the trivial case $\Phi = \nu \times 2\pi$, $\nu \in \mathbb{Z}$, commuting magnetic translation operators can be constructed if they enclose a so called super-cell on the lattice pierced by a magnetic flux equal to an integer multiple of 2π. For a super-cell of size $n_1 \times n_2$ the commutator vanishes if

$$[\hat{T}_1^M, \hat{T}_2^M] = 0 \quad \leftrightarrow \quad n_1 n_2 \Phi = 2\pi \frac{p}{q} n_1 n_2 = 2\pi \times \nu, \tag{18}$$

therefore $\frac{p}{q} n_1 n_2 \in \mathbb{Z}$. Choosing $n_1 = q$ and $n_2 = 1$ one can label the states with the eigenvalues of $\hat{T}_2^M$ and simultaneously with eigenvalues of $(\hat{T}_1^M)^q$. This states are Bloch eigenstates $\hat{H}|\vec{k}\rangle = E(\vec{k})|\vec{k}\rangle$, which satisfies

$$\hat{T}_1^q|\vec{k}\rangle = e^{iqk_1 a}|\vec{k}\rangle, \qquad \hat{T}_2|\vec{k}\rangle = e^{ik_2 a}|\vec{k}\rangle. \tag{19}$$

The momenta k_i are again periodic but in a range $-\frac{\pi}{aq} < k_1 \leq \frac{\pi}{aq}$ and $-\frac{\pi}{a} < k_2 \leq \frac{\pi}{a}$ parametrise the magnetic (BZ), which is again a torus but q times smaller, thus consist of $L_1 L_2/qa^2$ states. This leads to a decomposition of the spectrum into q different bands, which can be shown the following way:
Consider $\hat{T}_1^M|\vec{k}\rangle$. Since the magnetic translation operator commute with the Hamiltonian $[\hat{H}, \hat{T}_1^M] = 0$ the translated state is again an eigenstate of the Hamiltonian $\hat{H}\hat{T}_1^M|\vec{k}\rangle = E(\vec{k})|\vec{k}\rangle$. By use of eq.(19)

$$\hat{T}_2^M(\hat{T}_1^M|\vec{k}\rangle) = e^{i\Phi}\hat{T}_1^M\hat{T}_2^M|\vec{k}\rangle = e^{i(2\pi p/q + k_2 a)}\hat{T}_1^M|\vec{k}\rangle \tag{20}$$

$|\vec{k}\rangle$ has the same energy as $\hat{T}_1^M|\vec{k}\rangle \sim |(k_1, k_2 + 2\pi p/qa)\rangle$ and because of this it is q-times degenerated.

3.1. Anisotropic Hopfstadter model

The systems we are going to study consist of two dimensional, $w \times d$ square lattices with, lattice constant $a = 1$ and anisotropic hopping, varying t_y. Note: in the following computations the lattice consists of L nodes in x-direction numbered form zero to L-1 such that $w = a(L-1)$ see Fig.6.

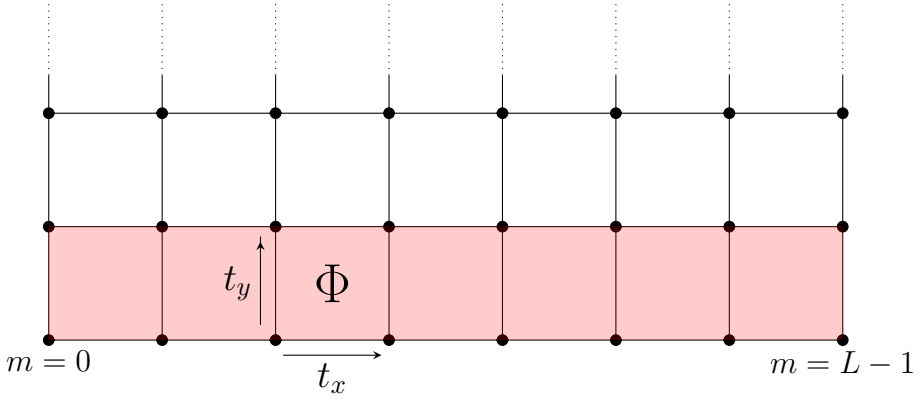

Figure 6: Schmatic drawing of the lattice. The red area denotes the area S spanned by the width and the distance between two adjacent conducting layers. In the case of a simple square lattice this area is given by $S = w \times a$

Studying such lattices is mostly done in the language of second-quantization, because of simpler handling. The zero field Hamiltonian is in second-quantization given by

$$\hat{H}_0 = -\sum_{m,n}\left(t_x\hat{a}^\dagger_{m+1,n}\hat{a}_{m,n} + t_y\hat{a}^\dagger_{m,n+1}\hat{a}_{m,n} + h.c.\right), \tag{21}$$

where $t_y/t_x = \kappa$ denotes the anisotropy. The magnetic translation operators are defined by

$$\hat{T}_x^0 = \sum_{m,n}\hat{a}^\dagger_{m+1,n}\hat{a}_{m,n}, \qquad \hat{T}_y^0 = \sum_{m,n}\hat{a}^\dagger_{m,n+1}\hat{a}_{m,n}. \tag{22}$$

Turn on a homogeneous magnetic field adds phase factors to the operators

$$\hat{T}_x = \sum_{m,n} \hat{a}^\dagger_{m+1,n}\hat{a}_{m,n}e^{i\phi^x_{m,n}}, \qquad \hat{T}_y = \sum_{m,n} \hat{a}^\dagger_{m,n+1}\hat{a}_{m,n}e^{i\phi^y_{m,n}}, \tag{23}$$

where $\phi^m_{m,n} = -\frac{e}{\hbar}A^m_{m,n}$, $m \in \{x, y\}$ is the Peierls phase. The phase eq.(13) is then given by

$$\gamma = \phi^x_{m,n} + \phi^y_{m+1,n} - \phi^x_{m,n+1} - \phi^y_{m,n}. \tag{24}$$

Defining the magnetic translation operators by constructing the phase $\theta^m_{m,n} = -\frac{e}{\hbar}\tilde{A}^m_{m,n}$

$$\hat{T}^M_x = \sum_{m,n} \hat{a}^\dagger_{m+1,n}\hat{a}_{m,n}e^{i\theta^x_{m,n}}, \qquad \hat{T}^M_y = \hat{a}^\dagger_{m,n+1}\hat{a}_{m,n}e^{i\theta^y_{m,n}}. \tag{25}$$

We want to proof eq.(18) and its consequence explicitly. To do this, the commutation relations $\left[\hat{T}^M_x, \hat{H}\right] = \left[\hat{T}^M_y, \hat{H}\right] = 0$, must be calculated.

$$\hat{H} = -\sum_{m,n}\left(t_x\hat{a}^\dagger_{m+1,n}\hat{a}_{m,n}e^{i\phi^x_{m,n}} + t_y\hat{a}^\dagger_{m,n+1}\hat{a}_{m,n}e^{i\phi^y_{m,n}} + h.c.\right). \tag{26}$$

Eq.(26) describes the Hamiltonian used in this calculations. A simple way of calculating such commutation relations is to let the commutator acting on a state $|m, n\rangle = \hat{a}^\dagger_{m,n}|0\rangle$.

$$\left[\hat{T}^M_y, \hat{H}\right]|m, n\rangle = -\left(t_x\left[\hat{T}^M_y, \hat{T}_x\right] + t_y\left[\hat{T}^M_y, \hat{T}_y\right]\right)|m, n\rangle, \tag{27}$$

where we can calculate the arising commutators separately.

$$\begin{aligned}
\left[\hat{T}^M_y, \hat{T}_x\right]|m, n\rangle &= \hat{T}^M_y\hat{T}_x|m, n\rangle - \hat{T}_x\hat{T}^M_y|m, n\rangle = \hat{T}^M_y e^{i\phi^x_{m,n}}|m+1, n\rangle - \hat{T}_x e^{i\theta^y_{m,n}}|m, n+1\rangle \\
&= e^{i(\phi^x_{m,n}+\theta^y_{m+1,n})}|m+1, n+1\rangle - e^{i(\theta^y_{m,n}+\phi^x_{m,n+1})}|m+1, n+1\rangle \\
&= e^{i(\phi^x_{m,n}+\theta^y_{m+1,n})}(1 - e^{i(\theta^y_{m,n}+\phi^x_{m,n+1}-\phi^x_{m,n}-\theta^y_{m+1,n})})|m+1, n+1\rangle \\
&= 0 \quad \rightarrow \quad \Delta_x\theta^y_{m,n} = \Delta_y\phi^x_{m,n} = \Delta_x\phi^y_{m,n} - \gamma
\end{aligned} \tag{28}$$

$$\begin{aligned}
\left[\hat{T}^M_y, \hat{T}_y\right]|m, n\rangle &= \hat{T}^M_y\hat{T}_y|m, n\rangle - \hat{T}_y\hat{T}^M_y|m, n\rangle = \hat{T}^M_y e^{i\phi^y_{m,n}}|m, n+1\rangle - \hat{T}_y e^{i\theta^y_{m,n}}|m, n+1\rangle \\
&= e^{i(\phi^y_{m,n}+\theta^y_{m,n+1})}|m, n+2\rangle - e^{i(\theta^y_{m,n}+\phi^y_{m,n+1})}|m, n+2\rangle \\
&= e^{i(\phi^y_{m,n}+\theta^y_{m,n+1})}(1 - e^{i(\theta^y_{m,n}+\phi^y_{m,n+1}-\phi^y_{m,n}-\theta^y_{m,n+1})})|m, n+2\rangle \\
&= 0 \quad \rightarrow \quad \Delta_y\theta^y = \Delta_y\phi^y
\end{aligned} \tag{29}$$

The commutation relations for the magnetic translation operator in x-direction are done the same way leading to the conditions $\Delta_x\theta^x_{m,n} = \Delta_x\phi^x_{m,n}$ and $\Delta_y\theta^x_{m,n} = \Delta_x\phi^y_{m,n} = \Delta_y\phi^x_{m,n} + \gamma$.

A solution which solves the above conditions is given by

$$\theta^x_{m,n} = \phi^x_{m,n} + \gamma \cdot n \qquad \theta^y_{m,n} = \phi^y_{m,n} - \gamma \cdot m. \tag{30}$$

Using this solution leads to eq.(18) and the associated conclusions. We will again choose Landau gauge. We define in the following the flux per plaquette as Φ, where we included the factor of 2π and write it in units of magnetic flux quanta. For a system with $L-1$ plaquettes it is given by

$$\Phi = 2\pi \frac{\phi}{L-1} = 2\pi \frac{p}{q}, \tag{31}$$

where ϕ is the total flux piercing S. Eq. (31) induces that the $\phi = (L-1)p/q$ has to be rational. Studying the system as a function of a continous field seems to lead to some difficulties because the also irrational values of ϕ are assumed. For irrational values there is no magnetic Brillouin zone and there are no distinct bands in the spectrum, instead it takes the form of a Cantor set. The question of applying the above formalism is correct even in this case was answered by D.R.Hofstadter [12], who has shown that it leads to the right physical result even in this case. In a very simple way one can argue that the set of irrationals numbers lies dense in the set of real numbers, such that one can replace the irrational flux by a rational flux that is arbitrary close to it. Changing ϕ, the size of the magnetic BZ and the number of distinct bands changes too, this will lead to special energy spectrum see Fig.7.

In Landau gauge the phases are give by $\phi^x_{m,n} = 0$ and $\phi^y_{m,n} = -2\pi \frac{\phi}{L-1} m$. To construct the new phases θ one has to look at the vector potential

$$\vec{A} = (0, Bm) \to \tilde{\vec{A}}(Bn, 0). \tag{32}$$

Therefore the new phases are defined by

$$\theta^x_{m,n} = -2\pi \frac{\phi}{L-1} n \qquad \theta^y_{m,n} = 0 \tag{33}$$

satisfying eq.(30). In this case the magnetic translation operators are defined

$$\hat{T}^x_{m,n} = \sum_{m,n} \hat{a}^\dagger_{m+1,n} \hat{a}_{m,n} e^{-i2\pi \frac{\phi}{L-1} n} \qquad \hat{T}^y_{m,n} = \sum_{m,n} \hat{a}^\dagger_{m,n+1} \hat{a}_{m,n}. \tag{34}$$

Approximate the irrational values of ϕ by rational ones then, by eq.(31) and eq.(18), the powers of translation operators can again be chosen $n_1 = q$ and $n_2 = 1$. Here it should be noted that every choice of n_1, n_2 that satisfies $n_1 n_2 = q$, is possible. The reason of choosing it this way is, that our system by it self depend specifically on the width and in y-direction just assume fully translational invariance. Thus it makes sense choosing the magnetic unit cell in the same manner $S_{muc} = q \times 1$

$$\left(\hat{T}^x_{m,n}\right)^{n_1} = \sum_{m,n} \hat{a}^\dagger_{m+q,n} \hat{a}_{m,n} e^{-i2\pi \frac{\phi}{L-1} qn} \qquad \left(\hat{T}^y_{m,n}\right)^{n_2} = \sum_{m,n} \hat{a}^\dagger_{m,n+1} \hat{a}_{m,n}. \tag{35}$$

It is obvious that then the operators commutate, because the picket up phase is an integer multiple of 2π

$$\frac{\phi}{L-1} qn = \frac{p}{q} qn = pn \in \mathbb{Z}, \tag{36}$$

since the site index n is clearly an integer. The first magnetic BZ is the given by $-\frac{\pi}{q} < k_x \leq \frac{\pi}{q}, \quad -\pi < k_y \leq \pi$.

To study the mesoscopic case we let the with L of the system be finite and the y-direction infinite. In the case where we will work with the Landauer Buettiker formalism this will be reached by attaching leads in y-direction. The Hamiltonian describing our system is given by

$$\boxed{\hat{H} = -\sum_{m,n} \left(t_x \hat{a}^\dagger_{m+1,n} \hat{a}_{m,n} + t_y \hat{a}^\dagger_{m,n+1} \hat{a}_{m,n} e^{i\Phi m} + h.c. \right)} \tag{37}$$

which is known as the famous **Harper-Hofstadter Hamiltonian**. Because in the case of interest $\kappa \ll 1$ it is called anisotropic. To study this case we will start with the isotropic one and take the limit to the anisotropic one. This allows us to get an understanding of how anisotropy affects the energy spectrum.

Plotting the spectrum of the above Hamiltonian as a function of magnetic flux will lead to the famous Hofstadter butterfly. The spectrum can be evaluated by calculating the eigenvalues of eq.(37) in Fourier space. Therefore one has to know the Fourier representation of the translation operators. Note: because the system is of finite length in x-direction, periodic boundary conditions and therefore Bloch like solutions can only be obtained in y-direction.

$$\begin{aligned} \hat{T}_x &= \sum_{m,n} \hat{a}^\dagger_{m+1,n} \hat{a}_{m,n} = \frac{1}{d} \sum_{m,n} \sum_{k_y,k'_y} e^{-ik_y n} e^{ik'_y n} \hat{c}^\dagger_{m+1,k_y} \hat{c}_{m,k'_y} \\ &= \sum_{m,n} \sum_{k_y,k'_y} \frac{1}{d} e^{in(k'_y - k_y)} \hat{c}^\dagger_{m+1,k_y} \hat{c}_{m,k'_y} \\ &= \sum_{m} \sum_{k_y,k'_y} \delta_{k_y,k'_y} \hat{c}^\dagger_{m+1,k_y} \hat{c}_{m,k'_y} = \sum_{m,k_y} \hat{c}^\dagger_{m+1,k_y} \hat{c}_{m,k_y}. \end{aligned} \tag{38}$$

We have set the lattice constant $a = 1$. For translation operator in y-direction one has to take care of the phase factor induced by the magnetic field.

$$\begin{aligned} \hat{T}_y &= \sum_{m,n} e^{-i\Phi m} \hat{a}^\dagger_{m,n+1} \hat{a}_{m,n} = \frac{1}{d} \sum_{m,n} \sum_{k_y,k'_y} e^{-ik_y(n+1)} e^{ik'_y n} e^{-i\Phi m} \hat{c}^\dagger_{m,k_y} \hat{c}_{m,k'_y} \\ &= \sum_{m} \sum_{k_y,k'_y} \delta_{k_y,k'_y} e^{-i(k_y+\Phi m)} \hat{c}^\dagger_{m,k_y} \hat{c}_{m,k'_y} = \sum_{m,k_y} e^{-i(k_y + 2\pi(\phi/(L-1))m)} \hat{c}^\dagger_{m,k_y} \hat{c}_{m,k_y}. \end{aligned} \tag{39}$$

In this form the Hamiltonian is given by an $L \times L$ matrix that reads

$$\boxed{H_{m,m} = -2t_y \cos\left(k_y + 2\pi \frac{\phi}{L-1} m \right), \quad H_{m+1,m} = H_{m,m+1} = -t_x} \tag{40}$$

The spectrum is then given by the eigenvalues of this Hamiltonian.

$$E(k_y)\begin{pmatrix}\psi_0\\ \psi_1\\ .\\ .\\ .\\ \psi_{L-1}\end{pmatrix} = H(k_y)\begin{pmatrix}\psi_0\\ \psi_1\\ .\\ .\\ .\\ \psi_{L-1}\end{pmatrix} \tag{41}$$

That is the Schroedinger equation associated with the Harper-Hofstadter Hamiltonian eq.37.

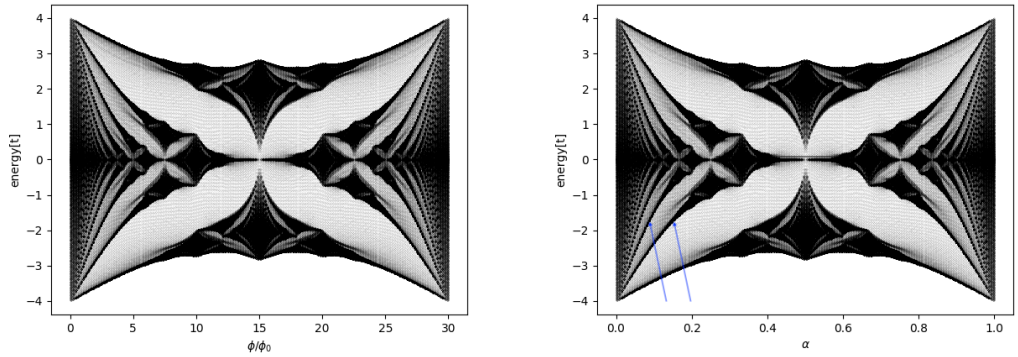

Figure 7: Spectrum of isotropic Harper Hofstadter Hamiltonian as a function of magnetic flux. The system size is given by $L = 30$. In the right plot, the parameter α denotes the ratio p/q. The blue arrows point out the Landau levels in the spectrum.

Observing the effect of anisotropy by a stepwise decrease of κ.

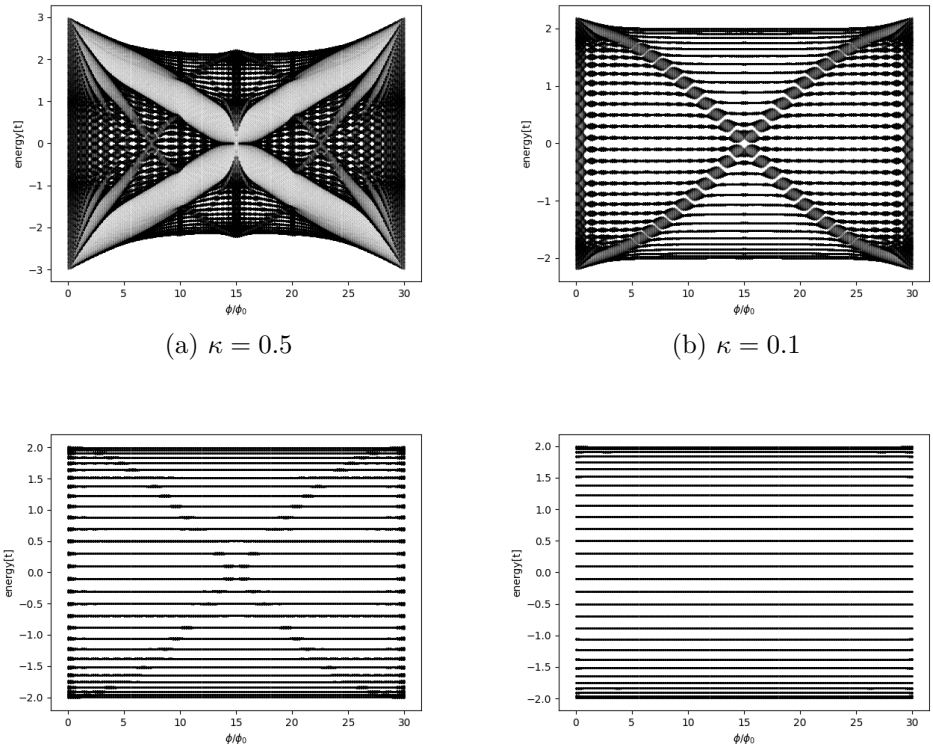

(a) $\kappa = 0.5$ (b) $\kappa = 0.1$

(c) $\kappa = 0.01$ (d) $\kappa = 0.001$

Figure 8: Spectrum of the anisotropic Hofstadter Hamiltonian as a function of magnetic flux. The subfigures **a,b,c,d** shows the spectrum for different anisotropy κ.

The form of the spectrum Fig.7 reminds to a butterfly and is therefore known as the Hofstadter butterfly. It reveals the effect of a magnetic field, combined with a periodic potential. Due to this interplay the spectrum decomposes into q bands, where each of it includes a large density of states. This q bands are the a Landau levels that are, for $\alpha = p/q$, p times degenerated.
Note: with just a magnetic field one would get the normal Landau quantization. Only the combination with a periodic potential leads to this fractionalized spectrum. The spectrum contains an inversions symmetry that is an effect of the particle-hole symmetry of the Harper-Hofstadter Hamiltonian [16].

If the hopping is turned into an anisotropic case $\kappa < 1$, the butterfly structure fan out. If $\kappa < 0.1$ only the big arms of the butterfly are visible and with further decreasing κ it fully disappears. This shows that the anisotropy reduces the effect of the magnetic field. Thus the lattice potential orders the states in discrete levels. These levels are not totally flat but shows a periodic broadening Fig.9, due to the effect of the magnetic field. We will see, that this behaviour is also reflected in the longitudinal transport.

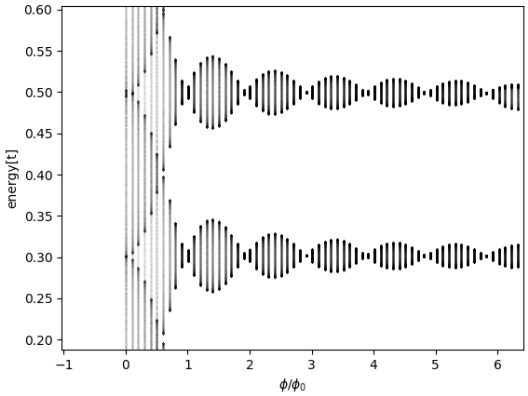

Figure 9: Zoom to two levels of the spectrum for an anisotropy of $\kappa = 0.1$.

The effect of the magnetic field goes in through the hopping in y-direction, which is affected also by the anisotropy. The question arises, if the effect of anisotropy would vanish, if the gauge would be chosen different $\phi^x_{m,n} = -\Phi n$. Before we give an answer to this question there is one point we have to check.

Eq.(41) seems to give L bands independent of ϕ. Looking at the spectrum Fig.7 this is clearly not the case. Taking the total flux $\phi \in [0, L-1]$ is equivalent to taking $\alpha = p/q \in [0, 1]$. Therefore every choice of q is indeed included in our model. The spectrum itself depends just on the value of α as a component of a periodic function. To check this, one can take the right figure of Fig.7 at an alpha value equal to $1/q$ and count the number of bands.

To answer the question above, we chose now the Landau gauge $\phi^x_{mn} = 2\pi\alpha n$. In this gauge the translation operators reads:

$$\hat{T}_y = \sum_{mn} \hat{a}^\dagger_{m,n+1}\hat{a}_{m,n} = \sum_{m,k_y} e^{-ik_y}\hat{c}^\dagger_{m,k_y}\hat{c}_{m,k_y} \tag{42}$$

$$\begin{aligned}\hat{T}_x &= \sum_{mn} e^{i2\pi\alpha n}\hat{a}^\dagger_{m+1,n}\hat{a}_{m,n} = \frac{1}{d}\sum_{m,n}\sum_{k_y,k'_y} e^{i2\pi\alpha n}e^{-ik_y n}e^{ik'_y n}\hat{c}^\dagger_{m+1,k_y}\hat{c}_{m,k'_y} \\ &= \sum_{m}\sum_{k_y,k'_y}\delta_{k'_y,k_y-2\pi\alpha}\hat{c}^\dagger_{m+1,k_y}\hat{c}_{m,k'_y} = \sum_{m}\sum_{k_y}\hat{c}^\dagger_{m+1,k_y}\hat{c}_{m,k_y-2\pi\alpha}.\end{aligned} \tag{43}$$

Using for the hermitian conjugate operator $\delta_{k'_y,k_y+2\pi\alpha}$, then the Hamiltonian is given by

$$\hat{H} = -\sum_{m,k_y} 2t_y\cos(k_y)\hat{c}^\dagger_{m,k_y}\hat{c}_{m,k_y} + t_x\left(\hat{c}^\dagger_{m+1,k_y-2\pi\alpha}\hat{c}_{m,k_y} + \hat{c}^\dagger_{m,k_y+2\pi\alpha}\hat{c}_{m,k_y}\right). \tag{44}$$

This Hamiltonian mixes k_y with $k_y \pm 2\pi\alpha$. We define $k_y = k'_y + 2\pi\alpha j$ and change to the first magnetic BZ as changing the borders of momentum space to $-\pi/q < k_y < \pi/q$.

Rewriting Eq. (44) this way on gets $H = \sum_{m,k'_y} H_m(k'_y)$, with

$$\begin{aligned}\hat{H}_m(k'_y) = &-\sum_{j=0}^{q-1} 2t_y \cos(k'_y + 2\pi\alpha j)\hat{c}^\dagger_{m,k'_y+2\pi\alpha j}\hat{c}_{m,k'_y+2\pi\alpha j} \\ &+ t_x\left(\hat{c}^\dagger_{m+1,k'_y+2\pi\alpha(j+1)}\hat{c}_{m,k'_y+2\pi\alpha j} + \hat{c}^\dagger_{m,k'_y+2\pi\alpha(j-1)}\hat{c}_{m+1,k'_y+2\pi\alpha j}\right).\end{aligned} \tag{45}$$

The rewritten Hamiltonian has the advantage that he does not couple different k'_y such that one can just study a particular block with fixed k'_y. This allows us to solve the Schroedinger equation as in eq.(41), that leads to the same butterfly spectrum as in Fig.7,8. To understand this one has to notice the following. In eq.(45) the magnetic field affects the spectrum the same way as before, as an additional argument of a periodic function. But with the difference that in this Hamiltonian, for every fixed k'_y, there is an additional q block over which j runs. The k'_y is an element of the first magnetic BZ, which is reduced to $-\pi/q < k'_y < \pi/q$. Thus, for each m, in total we have the same amount of arguments ranging from $-\pi$ to π that goes into the periodic function. Therefore affecting the spectrum the same way as in eq.(41) and is be itself affected the same way by anisotropy.

We can conclude that it does not depend on which Landau gauge we chose. In one case it affects the y-hopping directly by a flux dependent phase factor, in the other case it affects it by the flux dependent change of the BZ. In the following work we will only use the first gauge, as it is much simpler to work with it.

3.2. Bandstructure and density of states

To get further insights on has to study the bandstructure and density of states for specific magnetic flux and anisotropy. The calculation of the density of states (DOS) was done the following way

$$\rho(E) = \sum_{m,k_y} \delta(E - E_{m,k_y})) = \sum_{k_y} \mathrm{Tr}\left(\delta(E\mathbb{1} - H(k_y))\right), \tag{46}$$

where the delta function is approximated by

$$\delta(x) = \frac{1}{\pi}\lim_{\varepsilon\to 0}\frac{\varepsilon}{\varepsilon^2 + x^2}. \tag{47}$$

Note: the energy is in units of $t = t_x$. Unless there is not explicitly noted, all plots are done for $L = 50$ and $\epsilon = 0.01$.
Fig.10 shows the band structure and DOS for different anisotropy in the case of zero flux. It reveals that the anisotropy flattens the bands and in fact turns a continuous DOS to discrete peaks. The level spacing is getting smaller in the outer energy regions Fig.11. This leads to a domination of the DOS by this outer energy regions, when anisotropy is increasing. For larger systems the number of bands increases with L. The bands are filled in such a way that the level spacing in the outer energy regions shrinks faster then

the one in the middle of the spectrum. Due to this, the domination of the states from the outer energy region in the DOS is getting stronger.

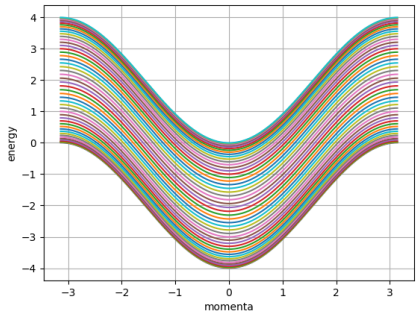

(a) $\kappa = 1$ (isotropic)

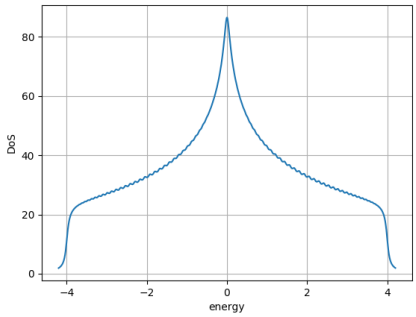

(b) $\kappa = 1$ (isotropic)

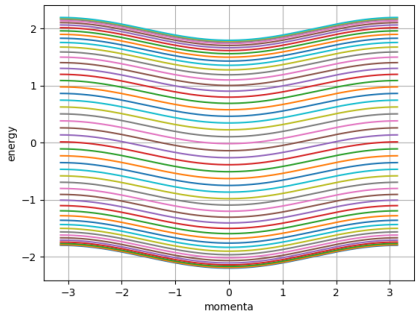

(c) $\kappa = 0.1$

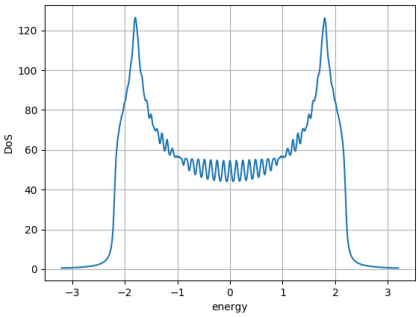

(d) $\kappa = 0.1$

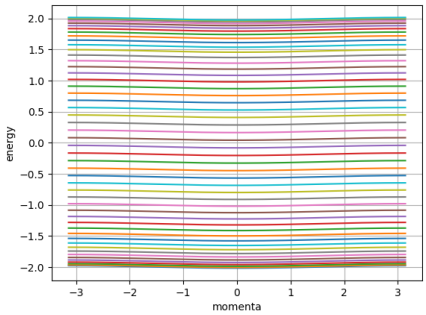

(e) $\kappa = 0.01$

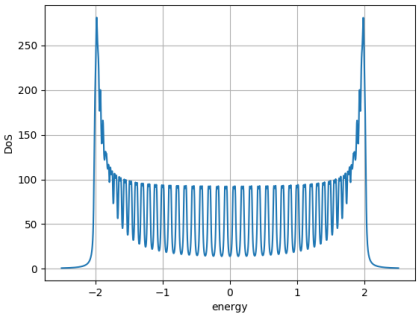

(f) $\kappa = 0.01$

Figure 10: Band structure and density of states for different anisotropy κ, without magnetic field.

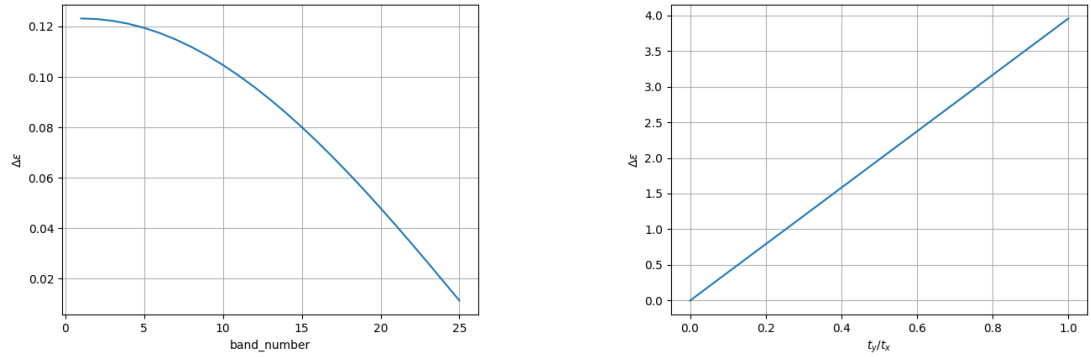

Figure 11: **Left**: energy difference between adjacent level as function of the level number. **Right**: energy difference between band edge and band bottom as function of κ.

Applying a magnetic field order the L energy bands into q bands, as noted in the chapters before. This is clearly visible in the band structure as well as in the density of states. Fig.12 shows the band structure and the DOS for the case of isotropic hopping and magnetic flux per plaquette given by $\Phi = \pi/6, \pi/3, \pi/2$, which corresponds to a q-band system with $q = 12, 6, 4$. By simple counting, the number of bands can be proven. In subfigure **c)** and **e)** the existence of edge states between the bands is observable. This gapless states consist of pairs of states that propagate in opposite directions and are well known form the physics of topological insulators [17]. For an even number of bands q the formation of Dirac cones was observed, with bulk Dirac points. The number of Dirac points is equal the number of bands q. For odd values the Dirac cones vanishes Fig.13. We will give a possible explanation of the missing of bulk Dirac points in this case. The number of bands q is equivalent to the number of lattice sites of which the hopping period is modelled and therefore to the size of the magnetic unit cell, as derived chapter 3.1. Thus the magnetic BZ is reduced by q. If the hopping period coincides with the lattice period a Dirac point is build. But because the greatest common divisor of two periods is two, the Dirac points arise always in pairs. Therefore, for an odd number of bands, the periods cannot coincide and no Dirac point is possible.

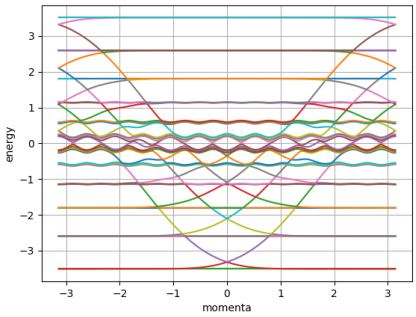

(a) $\Phi = \pi/6$

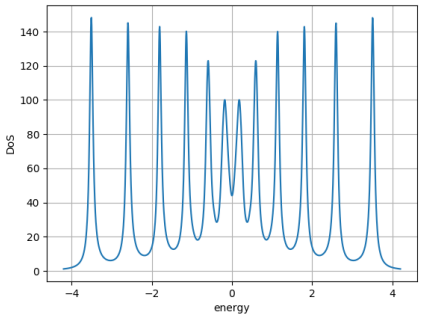

(b) $\Phi = \pi/6$

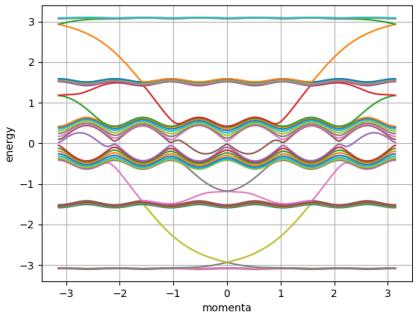

(c) $\Phi = \pi/3$

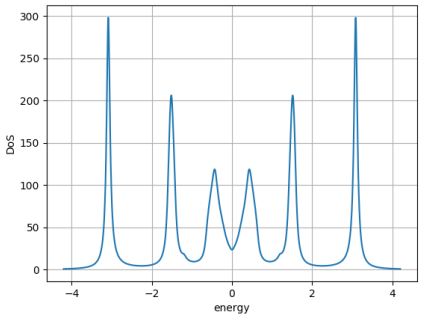

(d) $\Phi = \pi/3$

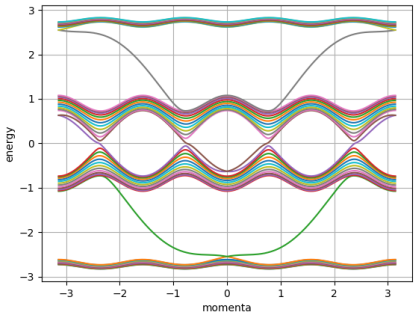

(e) $\Phi = \pi/2$

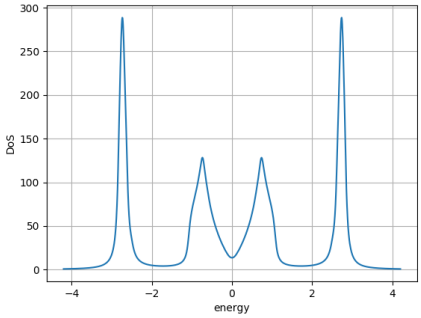

(f) $\Phi = \pi/2$

Figure 12: Band structure and density of states for an isotropic system, with different flux per plaquette Φ.

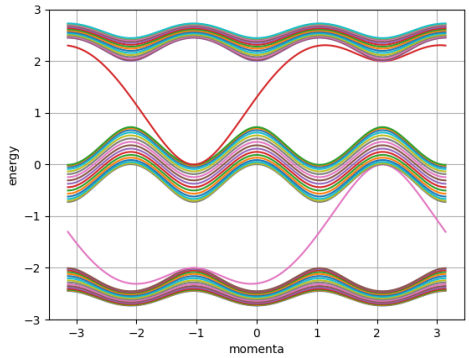

Figure 13: Band structure for an odd number of bands $q = 3$. For an odd value of q no Dirac cones can be observed.

Turning to the case of anisotropic hopping, as seen in the Hofstadter butterfly, the effect of the magnetic field is suppressed by the level spacing Fig.14. The edge states are more stable against the level spacing but also starts to disappear if the anisotropy is larger than $\kappa < 0.1$ Fig.15. This has a deep impact. The edge sates are related to the topology of a system, such that gaping this states is similar to changing the topology from a non-trivial one to a trivial one. That would be in the limit of large anisotropy $\kappa \to 0^+$ a trivial insulator in y-direction. This will have an effect on the transversal conductivity. Note: the edge states are not reflected in the discussion of the inter/intra-band Kubo formula and the Landauer approach, because there we only will consider longitudinal transport.

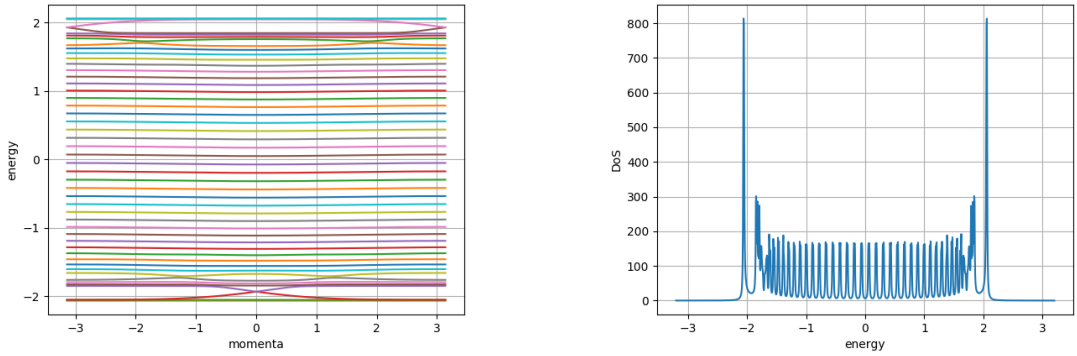

Figure 14: Band structure and density of states for anisotropic hopping $\kappa = 0.1$ and with a flux per plaquette of $\Phi = \pi/6$.

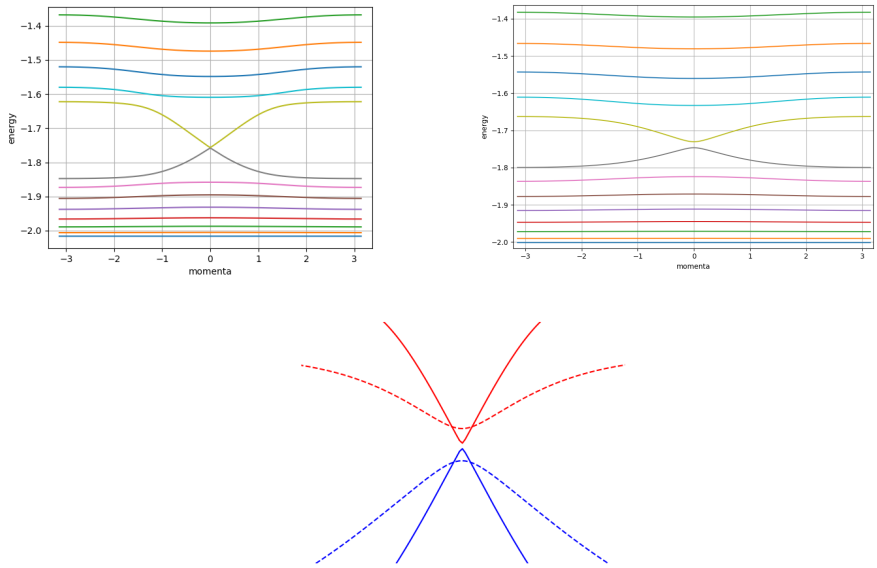

Figure 15: Splitting of the edge states as anisotropy is increased. The upper two plots are zoomed to the the edge states, for a anisotropy of $\kappa = 0.1, 0.05$ and flux per plaquette $\Phi = \pi/3$. The plot below shows the edge states for the two cases above, sketched as solid an dashed lines.

For increasing level number L, due to the reduced level spacing the gap gets closed again and the edge states remain. Fig.16 shows the effect of increasing L to the band structure at specific anisotropy. A flux of $\Phi = \pi/3$ implies $q = 6$, thus a six band model. In subfigure **a)** and **b)** one can observe that if the anisotropy is not to large, such that the band structure still remains, because of the higher level density the structure is getting clearer. Whereas in subfigure **c)** and **d)**, due to the large anisotropy the bands seems to hybridize in the limit of large L, resulting in an effective three band model. The question arises of what happens with the edge states in this case? To find an answer we will look at the transversal conductivity in section 8.3

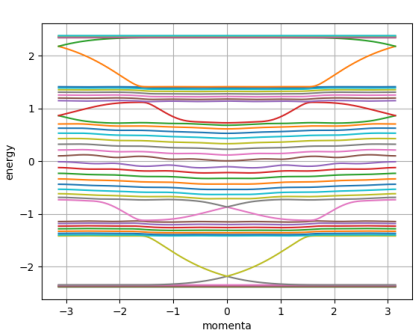

(a) $\kappa = 0.5$, $L = 50$

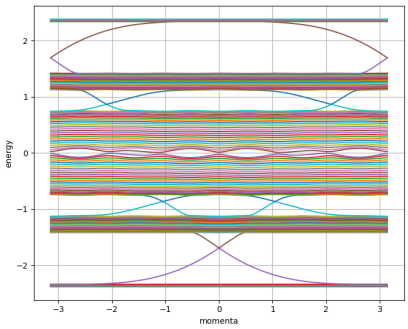

(b) $\kappa = 0.5$, $L = 150$

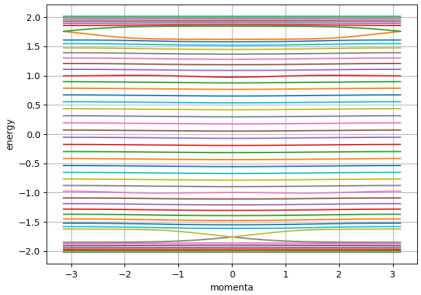

(c) $\kappa = 0.1$, $L = 50$

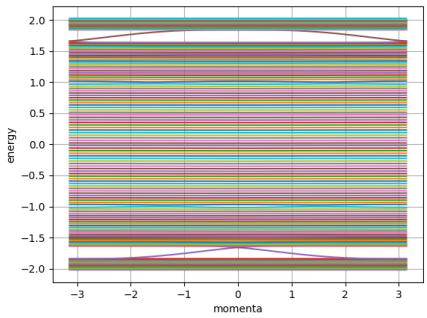

(d) $\kappa = 0.1$, $L = 150$

Figure 16: Effect of increasing level number L (increasing width) on the band structure, with a flux per plaquette of $\Phi = \pi/3$.

4. Landauer-Buettiker Formalism and Scattering Matrix

In Chapter 2.2, we have seen that mesoscopic transport is coherent if the size of the sample is smaller than the coherence length. Landauer and Buettiker developed a well elaborated framework for the description of such a transport [18].
Our system consist of a mesoscopic sample with disorder in it (scattering region) and attached leads see Fig.17. This leads connecting the scattering region to two electron reservoirs of specific chemical potentials. They are translational invariant. The mesoscopic system represents only a small perturbation to the reservoirs because of the much smaller conductor cross-section compared to the reservoir size. Therefore the reservoirs can be described in terms of an equilibrium state which is characterized by its chemical potential and temperature. The distribution of the electrons in the reservoirs are given by the Fermi-Dirac distribution function.

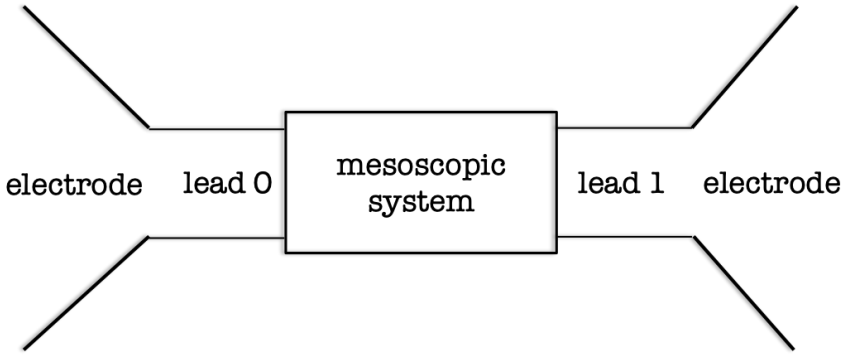

Figure 17: Mesoscopic sample, that is connected by the leads to two metallic electrodes. The chemical potential in the left electrode will be denoted as μ_0, the one in the right electrode as μ_1.

There are two main differences between the reservoirs and the mesoscopic sample that we want to emphasize here.

-) In the mesoscopic sample only elastic scattering processes occur whereas in the reservoir also inelastic does. This is because otherwise they could not establish an equilibrium state.

-) The mesoscopic system has a finite number of modes, whereas the reservoir has a large number of it, which lie energetically very close.

4.1. Landauer formalism

The leads connecting scattering region and reservoirs are ideal narrow channels, including well defined scattering states. Thus each state in lead n can be written as a product of a propagating wave in longitudinal direction and a stationary wave in the transverse direction [20]. To each longitudinal wave vector k there are $N_n(\varepsilon(k))$ transversal waves at energy $\varepsilon(k)$. This waves are called modes and their number depends on the width of

the system. In our case we have L transversal modes.

The Fermi distribution function, that describes the occupation of states, for an energy ε at temperature T in lead n is given by

$$f_n(\varepsilon) = \frac{1}{\exp((\varepsilon - \mu_n)/k_B T) + 1}. \tag{48}$$

For every energy ε the electrons occupy, in each of the $N(\varepsilon)$ transversal modes, negative and positive k states that corresponds to left and right moving states. Note: we analyse a system with two leads of equivalent geometry, therefore $N_0 = N_1 = N$. Consider the states moving from lead 0 to lead 1, that moves with the group velocity $v = \frac{1}{\hbar}\frac{\partial \varepsilon}{\partial k}$. This states carries the current

$$I^0_> = \sum_{k>0} env f_0(\varepsilon) = \frac{en}{\hbar} \sum_{k>0} \frac{\partial \varepsilon}{\partial k} f_0(\varepsilon) = \frac{2e}{h} \int_0^{+\infty} \frac{\partial \varepsilon}{\partial k} f_0(\varepsilon) dk = \frac{2e}{h} \int_{\varepsilon_0}^{+\infty} f_0(\varepsilon) d\varepsilon, \tag{49}$$

where we have used periodic boundary conditions in transport direction and spin degeneracy that brings in a factor of two. ε_0 defines the band bottom of the j band. Taking into account all transverse modes leads to

$$I^0_> = \frac{2e}{h} \int_{-\infty}^{+\infty} N(\varepsilon) f_0(\varepsilon) d\varepsilon. \tag{50}$$

On gets a similar expression for the current from lead 1 to lead 0. The current per unit energy can directly read off from eq.(50).

$$i^0_> = \frac{2e}{h} N(\varepsilon) f_0(\varepsilon), \qquad i^1_< = \frac{2e}{h} N(\varepsilon) f_1(\varepsilon). \tag{51}$$

Note: because we have assumed inelastic scattering in the reservoirs to reach thermal equilibrium, there are no reflected electrons. The ones enter lead 1 will disappear into the attached reservoir. Consider lead 0, there the total current per unity energy leaving the lead is given by $i^0 = i^0_> - i^0_<$. $i^0_<$ can be written in terms of the transmission amplitude $|t(\varepsilon)|^2$ as

$$i^0_< = (1 - |t(\varepsilon)|^2) i^0_> + |t(\varepsilon)|^2 i^1_<. \tag{52}$$

Under the consideration of current conservation we get

$$i^0 = i^1 = \frac{2e}{h} N(\varepsilon) |t(\varepsilon)|^2 (f_0(\varepsilon) - f_1(\varepsilon)). \tag{53}$$

Thus the full current is given by

$$I = \frac{2e}{h} \int_{-\infty}^{+\infty} T_{01}(\varepsilon)(f_0(\varepsilon) - f_1(\varepsilon)) d\varepsilon, \tag{54}$$

with the transmission function T_{01} between lead 0 and lead 1.

The conductance is defined as the quotient of current and voltage

$$G = \frac{I}{V_{bias}}, \tag{55}$$

where $V_{bias} = (\mu_0 - \mu_1)/e$ is the bias voltage given by the chemical potential difference of the reservoirs. In approximation of a small bias voltage, the conductance turns to

$$\boxed{\begin{aligned} G &= \frac{2e^2}{h}\int_{-\infty}^{+\infty} T_{01}(\varepsilon) \lim_{\mu_0\to\mu_1} \frac{(f(\varepsilon,\mu_0) - f(\varepsilon,\mu_1))}{\mu_0 - \mu_1} d\varepsilon \\ &= \frac{2e^2}{h}\int_{-\infty}^{+\infty} T_{01}(\varepsilon)\left(-\frac{\partial f(\varepsilon)}{\partial\varepsilon}\right) d\varepsilon. \end{aligned}} \tag{56}$$

For low temperature the derivative of the Fermi function is approximated by a delta distribution $\delta(\varepsilon - \varepsilon_F)$.
Here we have to give the following remark:
Eq.(56) is a linear response result. Only this case can be compared to the Kubo approach (see section 6), that is from the ground up a linear response result. For finite bias voltage, a linear approach is inadequate. Therefore we will in the following work only consider the linear case.

4.2. Scattering matrix

The scattering matrix S of a system, more precisely of its scattering region, relates the amplitudes of the incoming propagation modes to the ones of the outgoing modes, in all leads. We will now derive the scattering matrix for the system Fig.17, in the case with only one impurity located at $x = x_0$ and for just one of the L scattering channels (transversal modes). This small amount of impurity remains the mean free path long compared to the sample length, such that we are in the ballistic transport regime. We will see that starting from this case one can easily extend the result to systems with more impurities. The impurity is given by a delta-function multiplied with a potential U_0.
The equation of motion for the field operator of the electron is given by

$$i\hbar\partial_t\hat{\psi} = \left[\hat{\psi}, \hat{H}\right], \tag{57}$$

with the Hamiltonian

$$\hat{H} = \int_{-\infty}^{+\infty} \hat{\psi}^\dagger(x)\left(-\frac{\hbar^2}{2m}\frac{\partial^2}{\partial x} + U_0\delta(x - x_0)\right)\hat{\psi}(x)dx. \tag{58}$$

Using the anti-commutations relation for the field operators [19] to compute the commutator in eq.(57), leads to

$$i\hbar\partial_t\hat{\psi} = -\frac{\hbar^2}{2m}\left(\partial_x^2\hat{\psi}(x,t) - \tilde{U}_0\delta(x - x_0)\hat{\psi}(x,t)\right), \tag{59}$$

with $\tilde{U}_0 = U_0\dfrac{2m}{\hbar^2}$. We want to find a solution to eq.(59). From this equation one observes that $\hat{\psi}$ has to be continuous in x, whereas the derivative $\partial_x\hat{\psi}$ has a discontinuity at

$x = x_0$. This can be seen when integrating eq.(59) around this point.

$$\begin{aligned}\underbrace{\lim_{\varepsilon\to 0}\int_{x_0-\varepsilon}^{x_0+\varepsilon} i\hbar\partial_t\hat{\psi}}_{=0} &= -\lim_{\varepsilon\to 0}\int_{x_0-\varepsilon}^{x_0+\varepsilon}\frac{\hbar^2}{2m}\left(\partial_x^2\hat{\psi}(x,t) - \tilde{U}_0\delta(x-x_0)\hat{\psi}(x,t)\right) \\ &= -\frac{\hbar^2}{2m}\lim_{\varepsilon\to 0}\left(\partial_x\hat{\psi}(x+\varepsilon,t) - \partial_x\hat{\psi}(x-\varepsilon,t)\right) - U_0\hat{\psi}(x_0,t).\end{aligned} \tag{60}$$

Thus we get the three conditions

$$i\hbar\partial_t\hat{\psi}(x,t) = -\frac{\hbar^2}{2m}\partial_x^2\hat{\psi}(x,t) \qquad x \neq x_0 \tag{61}$$

$$\lim_{\varepsilon\to 0}\left(\hat{\psi}(x+\varepsilon,t) - \hat{\psi}(x-\varepsilon,t)\right) = 0 \tag{62}$$

$$\lim_{\varepsilon\to 0}\left(\partial_x\hat{\psi}(x+\varepsilon,t) - \partial_x\hat{\psi}(x-\varepsilon,t)\right) - U_0\hat{\psi}(x_0,t) = 0. \tag{63}$$

These equations can be solved by the following Ansatz

$$\hat{\psi}_k(x,t) = e^{-i\varepsilon_k t/\hbar}\begin{cases}\hat{a}_{0k}e^{ikx} + \hat{b}_k e^{-ikx} & x < x_0 \\ \hat{b}_{1k}e^{ikx} + \hat{a}_{1k}e^{-ikx} & x > x_0\end{cases}, \tag{64}$$

where $\varepsilon_k = \frac{\hbar^2 k_x^2}{2m}$ and $\hat{a}_{0/1}, \hat{b}_{0/1}$ denotes the amplitude operators of lead 0 ($x < x_0$) and lead 1 ($x > x_0$). The solution of this set of linear equations for the amplitude operators is given by the so called transfer matrix

$$\begin{pmatrix}\hat{b}_{1k}\\ \hat{a}_{1k}\end{pmatrix} = M_k\begin{pmatrix}\hat{a}_{0k}\\ \hat{b}_{0k}\end{pmatrix}, \tag{65}$$

with

$$M_k = \begin{pmatrix}1 + \frac{U_0}{2ik} & \frac{U_0}{2ik}e^{-2ikx_0} \\ -\frac{U_0}{2ik}e^{2ikx_0} & 1 - \frac{U_0}{2ik}\end{pmatrix}. \tag{66}$$

This matrix connect the amplitude operators in lead 0 to the ones in lead 1 and describes how they are transferred. This matrix satisfies the properties $detM_k = 1$, $M_{21} = M_{12}^*$. Most of the time one is more interested in expressing the outgoing state operators as a function of the incoming state operators. Then one has to use the scattering matrix instead of the transfer matrix.

$$\begin{pmatrix}\hat{b}_{0k}\\ \hat{b}_{1k}\end{pmatrix} = S_k\begin{pmatrix}\hat{a}_{0k}\\ \hat{a}_{1k}\end{pmatrix}, \tag{67}$$

where the S-matrix is given in terms of the transfer matrix

$$S = \begin{pmatrix}r & t'\\ t & r'\end{pmatrix} = \frac{1}{M_{22}}\begin{pmatrix}-M_{21} & 1\\ 1 & M_{12}\end{pmatrix}. \tag{68}$$

The coefficients t, t', r, r' are the transmission and reflection amplitudes. For example if one has an incoming wave from the left, then

$$\begin{aligned} T &= |t|^2 = \left|\frac{1}{M_{22}}\right|^2 \\ R &= |r|^2 = \left|-\frac{M_{21}}{M_{22}}\right|^2 = \left|\frac{M_{12}}{M_{22}}\right|^2 . \end{aligned} \tag{69}$$

The scattering matrix has the following main properties:

-) flux conservation $S^\dagger(E) = S(E)$

-) time reversal symmetry $S^\dagger_{ij}(E, B) = S_{ij}(E, -B)$

Because of the linearity of the transfer matrix, the case of one impurity can easily be expanded to the case of many impurities. As an example we take the case of two impurities at x_1, x_2 then the transfer matrix is given by $M_k = M_k(x_1) \cdot M_k(x_2)$.
Knowing the scattering matrix one can directly calculate the transmission function for an arbitrary number of leads and channels, by a simple summation.

$$T_{nm}(E) = \sum_{j\in m}\sum_{i\in n} |t_{ij}(E)|^2 = \sum_{j\in m}\sum_{i\in n} |S_{ij}(E)|^2, \tag{70}$$

where n,m denotes the leads and i,j sums over the transverse modes in each lead.

5. Kubo-Formalism

When studying systems in the ground state, a lot of information is provided by the linear response to an external perturbation, that can be characterized by a constant coefficient. In 1957 R.Kubo [23] did a first approach to derive such linear response coefficients. His formalism is based on the linear response of a system in equilibrium, to a small external perturbation. The response can be expressed as fluctuations of the dynamical variables, of the unperturbed system. That means a correlation function, a tensor quantity, that consist of the response coefficients, describing the linear response. In the case of electronic transport due to an external electromagnetic field this correlation function is the conductivity.
Such an electromagnetic field is uniquely described by a vector potential $\vec{A}(\vec{r},t)$ and a scalar potential $\Phi(\vec{r},t)$. For the upcoming calculations we have chosen the gauge

$$\vec{A}(t) = -i\frac{c}{\omega + i\eta}\vec{E}_0 e^{-i(\omega+i\eta)t}, \qquad \Phi(\vec{r},t) = 0, \tag{71}$$

where we have neglected the position dependence, which is justified if the wave length of the field is large compared to the lattice constant. Although we are interested in DC electric field, it is simpler to work with an AC electric field and at the end take the DC limit $\omega \to 0$. The term η was introduced to satisfy causality. In chapter 5.3 we will discuss this term in more detail.
The following important remark should be done her. The system we will analyse is under the influence of a homogeneous magnetic field. This by itself bring in a minimal coupling to the vector potential describing the magnetic field, but that is included in our momentum $\vec{p}$. The unperturbed Hamiltonian H_0 already includes the magnetic field, like a Hall system, and therefore the additional potential is just describing the external electrical field. Of course if we want to use the Kubo formula at the end we have to write the correct current operator. The field couples to the charged particles with minimal coupling $\vec{p} \to \vec{p} - \frac{e}{c}\vec{A}(t)$. The coupling leads to the N-particle Hamiltonian in first quantization calculated in [9], which is given by

$$\begin{aligned} H &= H_0 + H_{int} \\ &= H_0 + \int d^3r' \left[-\frac{1}{c}\vec{j}(\vec{r}')\vec{A}(t) + \frac{e^2}{2mc^2} n(\vec{r}')\vec{A}^2(t) \right], \end{aligned} \tag{72}$$

with the current and particle density operator defined by

$$\vec{j}(\vec{r},t) = \frac{e}{2m}\sum_{i=1}^{N}\left[\vec{p}_i\delta(\vec{r}-\vec{r}_i) + \delta(\vec{r}-\vec{r}_i)\vec{p}_i\right], \qquad n(\vec{r}) = \sum_{i=1}^{N}\delta(\vec{r}-\vec{r}_i). \tag{73}$$

The coupling of the em-field in this way, where spin contributions are neglected is called diamagnetic coupling. To study transport properties, the expectation value of the full current operator is needed

$$\vec{J}(\vec{r},t) = \frac{e}{2m}\sum_{i=1}^{N}\left[\left(\vec{p}_i - \frac{e}{c}\vec{A}(t)\right)\delta(\vec{r}-\vec{r}_i) + \delta(\vec{r}-\vec{r}_i)\left(\vec{p}_i - \frac{e}{c}\vec{A}(t)\right)\right]. \tag{74}$$

The expectation value of the current operator can be written as

$$\begin{aligned}\langle J\rangle_{\rho(t)} &= Tr\{\rho_0 J\} - \frac{i}{\hbar}\int_{-\infty}^{t} dt' Tr\left\{e^{-i/\hbar H_0 t}[H_{int}(t'),\rho_0]e^{i/\hbar H_0 t}J\right\} \\ &= \langle J\rangle_{\rho_0} - \frac{i}{\hbar}\int_{-\infty}^{t} dt' Tr\left\{[H_{int}(t'),\rho_0]e^{i/\hbar H_0 t}Je^{-i/\hbar H_0 t}\right\} \\ &= \langle J\rangle_{\rho_0} - \frac{i}{\hbar}\int_{-\infty}^{t} dt' Tr\left\{\rho_0[\tilde{J}(t),H_{int}(t')]\right\} \\ &= \langle J\rangle_{\rho_0} - \frac{i}{\hbar}\int_{-\infty}^{t} dt' \left\langle[\tilde{J}(t),H_{int}(t')]\right\rangle_{\rho_0},\end{aligned} \tag{75}$$

where $\tilde{J}$ is the current operator in the interaction picture and ρ the density matrix approximated by

$$\rho(t) \approx \rho_0 - \frac{i}{\hbar}\int_{-\infty}^{t} dt' e^{-i/\hbar H_0 t}[H_{int}(t'),\rho_0]e^{i/\hbar H_0 t}. \tag{76}$$

The derivation of eq.(76) can be found in [15].

Evaluating the the current operator eq.(74) this way one gets to linear order

$$\langle J_\alpha(\vec{r})\rangle_{\rho(t)} = \frac{-e^2}{mc}A_\alpha(t)\langle n(\vec{r})\rangle_{\rho_0} + \int d^3r' \int dt \left[\frac{-1}{c}\sum_{\beta=1}^{3}\chi_{j_\alpha(\vec{r}),j_\beta(\vec{r}')}(t-t')A_\beta(t')\right] \tag{77}$$

with the retarded susceptibility

$$\chi_{j_\alpha(\vec{r}),j_\beta(\vec{r}')} = \frac{i}{\hbar}\left\langle[j_\alpha(\vec{r},t),j_\beta(\vec{r}',t')]\right\rangle_{\rho_0}\theta(t-t'). \tag{78}$$

Note: the first term in eq.(77) is due to the fact that the full current operator itself include the vector potential. It is called the diamagnetic term of the current. The consecutive terms are non-equilibrium terms given by the linear response of an external field. On conclude that the em-field couples to the system by the current and particle density operator.

Because we are interested in the electrical conductivity where the electric field is independent of the position in space eq.(71), we will work with expectation values averaged over the whole system.

$$\left\langle\vec{J}\right\rangle = \frac{1}{V}\int d^3r \left\langle J(\vec{r})\right\rangle \quad \text{and} \quad \langle n\rangle = \frac{1}{V}\int d^3r \left\langle n(\vec{r})\right\rangle. \tag{79}$$

With respect to that assumption, the expectation value of the current operator in eq.(77) becomes

$$\langle J_\alpha\rangle = i\frac{ne^2}{m(\omega+i\eta)}E_\alpha e^{-i(\omega+i\eta)t} - \frac{i}{(\omega+i\eta)V}\sum_{\beta=1}^{3}\chi_{j_\alpha j_\beta}(\omega+i\eta)E_{0\beta}e^{-i(\omega+i\eta)t}. \tag{80}$$

The conductivity tensor can directly read out from eq.(80)

$$\boxed{\sigma_{\alpha,\beta}(\omega+i\eta)=\frac{-i}{(\omega+i\eta)V}\chi_{j_\alpha j_\beta}(\omega+i\eta)+i\frac{ne^2}{m(\omega+i\eta)}\delta_{\alpha,\beta}}. \tag{81}$$

This formula is known as the **Kubo formula for conductivity**, consisting of two parts $\sigma^{(1)}_{\alpha\beta}+\sigma^{(dia)}\delta_{\alpha\beta}$.

5.1. Representation in many-body basis

By taking a many-particle basis $|n\rangle$ of H_0 one can rewrite the Fourier transformed susceptibility [9] to get

$$\sigma^{(1)}_{\alpha\beta}(\omega)=\frac{i}{\omega+i\eta}\frac{1}{VZ_0}\sum_{n,m}\frac{\langle n|\hat{j}_\alpha|m\rangle\langle m|\hat{j}_\beta|n\rangle}{\hbar\omega+\varepsilon_n-\varepsilon_m+i\eta}\left(e^{-\beta\varepsilon_n}-e^{-\beta\varepsilon_m}\right), \tag{82}$$

with the partition function $Z_0=\sum_n e^{-\beta\varepsilon_n}$. Because the quantities we measure are always real, we will calculate the real part of the conductivity $\mathrm{Re}\,\sigma_{\alpha\beta}(\omega)=\mathrm{Re}\,\sigma^{(1)}_{\alpha\beta}(\omega)$, using $\frac{1}{(a+i\eta)}=\frac{1}{a}-i\pi\delta(a)$.

$$\mathrm{Re}\,\sigma^{(1)}_{\alpha\beta}=\frac{\pi}{V\omega Z_0}\sum_{n,m}\langle n|\hat{j}_\alpha|m\rangle\langle m|\hat{j}_\beta|n\rangle\delta(\hbar\omega+\varepsilon_n-\varepsilon_m)\left(e^{-\beta\varepsilon_n}-e^{-\beta\varepsilon_m}\right), \tag{83}$$

with the current operator expressed in a single particle basis $\hat{j}=\sum_{i,l}\frac{e}{m}\langle i|\hat{p}|l\rangle\hat{c}^\dagger_i\hat{c}_l$ it can be written as

$$\frac{\pi e^2}{V\omega m^2}\sum_{i,l,j,q}\langle i|\hat{p}_\alpha|l\rangle\langle j|\hat{p}_\beta|q\rangle\frac{1}{Z_0}\sum_{n,m}\delta(\hbar\omega+\varepsilon_n-\varepsilon_m)\langle n|\hat{c}^\dagger_i\hat{c}_l|m\rangle\langle m|\hat{c}^\dagger_j\hat{c}_q|n\rangle\left(e^{-\beta\varepsilon_n}-e^{-\beta\varepsilon_m}\right). \tag{84}$$

The delta distribution gives a condition for the energies and therefore a condition on indices counting in the sum. We rewrite the sum as $\sum'_{n,m}$ that only runs over energies satisfying the delta distribution. Calculation of this sum, using the anticommutaion relation for Fermions, gives

$$\delta'_{lj}\delta'_{iq}\left(f(\varepsilon_i)-f(\varepsilon_l)\right)\to\delta_{lj}\delta_{jk}\delta(\hbar\omega+\varepsilon_i-\varepsilon_l)\left(f(\varepsilon_i)-f(\varepsilon_l)\right). \tag{85}$$

Then the real part is given by

$$\frac{\pi}{V\omega}\sum_{l,q}\langle q|\hat{j}_\alpha|l\rangle\langle l|\hat{j}_\beta|q\rangle\delta(\hbar\omega+\varepsilon_q-\varepsilon_l)\left(f(\varepsilon_k)-f(\varepsilon_l)\right). \tag{86}$$

Note: the delta distribution replaces the frequency in the denominator as $\omega=(\varepsilon_l-\varepsilon_q)/\hbar$. Taking the limit for small frequencies leads to the DC conductivity. The full complex conductivity can therefore be written as

$$\boxed{\sigma_{\alpha\beta}=\frac{i\hbar}{V(\omega+i\eta)}\sum_{l,q}\langle q|\hat{j}_\alpha|l\rangle\langle l|\hat{j}_\beta|q\rangle\frac{f(\varepsilon_q)-f(\varepsilon_l)}{\varepsilon_q-\varepsilon_l+i\eta}+i\frac{ne^2}{m(\omega+i\eta)}\delta_{\alpha\beta}} \tag{87}$$

For the DC and longitudinal conductivity $\alpha = \beta$ one can prove that the imaginary part of $\sigma^{(0)}_{\alpha\alpha}$ compensate the diamagnetic contribution [9], therefore we can neglect it. We want to study longitudinal transport in y-direction of 2-dim systems, thus eq.(87) can be written as

$$\begin{aligned} \mathrm{Re}\,\sigma^{DC}_{yy} &= \frac{\pi\hbar}{V}\sum_{q,l}|\langle q|\hat{j}_y|l\rangle|^2\frac{f(\varepsilon_q)-f(\varepsilon_l)}{\omega}\delta(\varepsilon_q-\varepsilon_l) \\ \rightarrow \sigma^{DC}_{yy} &= \frac{i\hbar}{V}\sum_{q,l}\frac{f(\varepsilon_q)-f(\varepsilon_l)}{\varepsilon_l-\varepsilon_q}\frac{|\langle q|\hat{j}_y|l\rangle|^2}{\varepsilon_q-\varepsilon_l+i\eta}. \end{aligned} \tag{88}$$

Working explicitly with a Bloch basis in y-direction $|q\rangle = |nk'_y\rangle$, $|l\rangle = |mk_y\rangle$, the expectation value of the current operator becomes

$$\begin{aligned} \langle nk'_y|\hat{j}_y|mk_y\rangle &= \frac{e}{iVm}\int dy e^{-ik'_y y}u^*_{nk'_y}(y)\partial_y e^{ik_y y}u_{mk_y}(y) \\ &= \frac{e}{imN}\sum_{R_y}e^{i(k_y-k'_y)R_y}\frac{1}{V_{uc}}\int_{uc}dy u^*_{nk'_y}(y)e^{i(k_y-k'_y)y}(\partial_y+ik_y)u_{mk_y}(y) \\ &= \delta_{k_y k'_y}\frac{1}{V_{uc}}\int_{uc}dy u^*_{nk'_y}(y)(p_y+k_y)u_{mk_y}(y). \end{aligned} \tag{89}$$

Because of the current expectation value, the momentum has to be the same and the states only differ by its band index. Including the geometry of our system where $V = L\cdot d$ and replacing the sum over momenta by an integral, one gets

$$\sum_{q,l} \rightarrow \sum_{n,m}^{L}\sum_{k_y} \rightarrow d\sum_{n,m}\int_{-\pi}^{\pi}\frac{dk_y}{2\pi}. \tag{90}$$

By the use of this, eq.(88) can be written as [5]

$$\boxed{\sigma^{DC}_{yy} = \frac{i\hbar}{L}\sum_{n,m}^{L}\int_{-\pi}^{\pi}\frac{dk_y}{2\pi}\left(\frac{f(\varepsilon_n)-f(\varepsilon_m)}{\varepsilon_m-\varepsilon_n}\right)\frac{|\langle n|\hat{j}_y|m\rangle|^2}{\varepsilon_n-\varepsilon_m+i\eta}} \tag{91}$$

The explicit intra-band formula is given when choosing equal bands $n = m$ in eq.(91). Then $\varepsilon_m - \varepsilon_n \rightarrow 0$ and therefore the difference of the Fermi distributions turns into a derivative of it.

$$\boxed{\sigma^{DC}_{yy}(n=m) = \frac{\hbar}{L\eta}\sum_{n}\int_{-\pi}^{\pi}\frac{dk_y}{2\pi}\left(-\frac{\partial f(\varepsilon_n)}{\partial\varepsilon_n}\right)|\nu^y_n|^2} \tag{92}$$

Remark: eq.(91) expresses the conductivity in terms of eigenvalues and eigenvectors of the Hamiltonian. For a general Hamiltonian, these can be difficult to obtain, therefore it is in such cases convenient to write the conductivity in a representation free way see Appendix B.

5.2. Kubo formalism for transversal conductivity

The Kubo formula for the the quantum Hall effect is given by [30]

$$\begin{aligned}\sigma_{kl} = &\frac{ie^2\hbar}{L}\sum_{\alpha}\sum_{\beta\neq\alpha}(f_\alpha - f_\beta)\frac{\langle\alpha|\hat{\nu}_k|\beta\rangle\langle\alpha|\hat{\nu}_l|\beta\rangle}{(\varepsilon_\alpha-\varepsilon_\beta)^2+\eta^2}\\ &+\frac{e^2\hbar}{L}\sum_{\alpha}\sum_{\beta\neq\alpha}\left(\frac{f_\alpha-f_\beta}{\varepsilon_\alpha-\varepsilon_\beta}\right)\frac{\eta}{(\varepsilon_\alpha-\varepsilon_\beta)^2+\eta^2}\langle\alpha|\hat{\nu}_k|\beta\rangle\langle\beta|\hat{\nu}_l|\alpha\rangle,\end{aligned} \tag{93}$$

where α, β denotes the eigenstates of the lattice Hamiltonian eq.(37). We used, that the expectation values of the current operators, for different states, are purely imaginary and expressed them in terms of the velocity operator

$$\langle\alpha|\hat{j}_x|\beta\rangle\langle\beta|\hat{j}_y|\alpha\rangle = e^2\hbar\langle\alpha|\hat{\nu}_x|\beta\rangle\langle\beta|\hat{\nu}_y|\alpha\rangle. \tag{94}$$

The velocity operator is equal to the time derivative of the displacement operator $\hat{u}_k$, $k\in\{x,y\}$ whose time evolution is given by the Heisenberg equation

$$\hat{\nu}_k = \frac{d}{dt}\hat{u}_k = \frac{1}{i\hbar}[\hat{u}_k,\hat{H}]. \tag{95}$$

Taking the Hamiltonian defined eq.(37), the velocity operators are given by

$$\begin{aligned}\hat{\nu}_x &= -\frac{it_x}{\hbar}\sum_{m,n}\left(\hat{c}^\dagger_{m,n}\hat{c}_{m+1,n}-\hat{c}^\dagger_{m+1,n}\hat{c}_{m,n}\right)\\ \hat{\nu}_y &= -\frac{it_y}{\hbar}\sum_{m,n}\left(\hat{c}^\dagger_{m,n}\hat{c}_{m,n+1}e^{-i\Phi m}-\hat{c}^\dagger_{m,n+1}\hat{c}_{m,n}e^{i\Phi m}\right).\end{aligned} \tag{96}$$

As before we will apply periodic boundary conditions in y-direction. Then the operators are given by

$$\begin{aligned}\hat{\nu}_x &= -\frac{it_x}{\hbar}\sum_{m,k_y}\left(\hat{c}^\dagger_{m,k_y}\hat{c}_{m+1,k_y}-\hat{c}^\dagger_{m+1,k_y}\hat{c}_{m,k_y}\right)\\ \hat{\nu}_y &= \frac{it_y}{\hbar}\sum_{m,k_y}2\sin\left(k_y+2\pi\frac{\Phi_{tot}}{L}m\right)\hat{c}^\dagger_{m,k_y}\hat{c}_{m,k_y}.\end{aligned} \tag{97}$$

Thus the velocity operator in y-direction can be expressed as $\hat{\nu}_y = \partial\hat{H}/\partial k_y$. Calculation of the expectation value for the y-current operator for $|\alpha\rangle = |m,k_y\rangle$, $|\beta\rangle = |m',k'_y\rangle$ leads to

$$\begin{aligned}\langle m,k_y|\partial_y\hat{H}|m',k'_y\rangle &= \langle m,k_y|(\partial_y\hat{H}|m',k'_y\rangle) - \langle m,k_y|\hat{H}\partial_y|m',k'_y\rangle\\ &= (\varepsilon_m(k_y)-\varepsilon_{m'}(k'_y))\langle m,k_y|\partial_y|m',k'_y\rangle\delta_{k_y,k'_y},\end{aligned} \tag{98}$$

where the same procedure as in eq.(89) was used. Using this, one gets the final expression for the conductivity

$$\sigma_{xy} = \frac{ie^2\hbar}{L}\sum_m\sum_{m'\neq m}\int\frac{dk_y}{2\pi}(f(\varepsilon_m(k_y)) - f(\varepsilon_{m'}(k_y)))\frac{\langle m,k_y|\hat{\nu}_x|m',k_y\rangle\langle m',k_y|\hat{\nu}_y|m,k_y\rangle}{(\varepsilon_m(k_y)-\varepsilon_{m'}(k_y))^2+\eta^2}$$
$$\sigma_{yy} = \frac{e^2\hbar\eta}{L}\sum_m\sum_{m'\neq m}\int\frac{dk_y}{2\pi}\left(\frac{f(\varepsilon_m(k_y)) - f(\varepsilon_{m'}(k_y))}{\varepsilon_m(k_y)-\varepsilon_{m'}(k_y)}\right)\frac{|\langle m,k_y|\hat{\nu}_y|m',k_y\rangle|^2}{(\varepsilon_m(k_y)-\varepsilon_{m'}(k_y))^2+\eta^2} \tag{99}$$

We can observe that the longitudinal conductance in the quantum Hall case is equivalent to the inter band conductance.

5.3. Physical meaning of η

We introduced the term η in eq.(71) to satisfy causality. If one is using counter integration techniques to derive the Kubo formula, one can see that η shift the poles form real axis in the complex plane and one can use the residue theorem, as for example in [24]. Taking η this way, one has to take the limit $\eta \to 0^+$. But that leads to a divergence of the intra-band Kubo formula eq.(92). In [25] G.Czycholl and B.Kramer have shown that introducing such a parameter, the limit to zero has to be done after the thermodynamic limit. But study finite systems, like the dalfossites in [5] that have a width of $L \approx 8000$, it would still diverge. Even if this parameter has just the function of letting the model converge, the question of the correct value in the finite case remains.

It is obvious that intra-band contribution scales as $1/\eta$. To see how the inter-band contribution scales, we calculated it at different Fermi energies, as a function of η Fig.18.

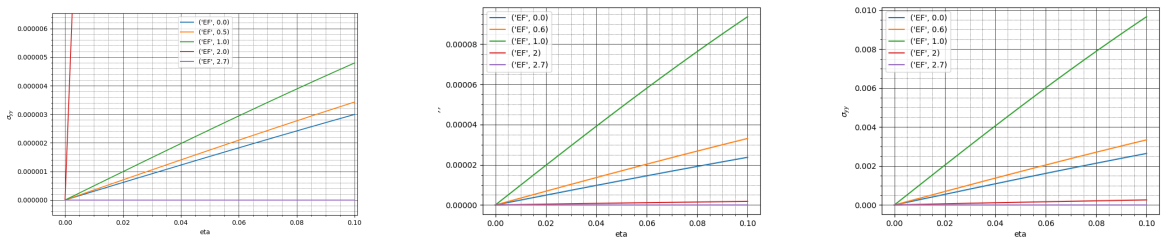

Figure 18: Inter-band conductivity as function of η, at different Fermi energies. **Left**: $\Phi = \pi/10$, $\kappa = 0.01$. **Middle**: $\Phi = \pi/4$, $\kappa = 0.01$. **Right**: $\Phi = \pi/4$, $\kappa = 0.1$

In Fig.18, one can observe that the inter-band conductivity increases nearly linear for all values of the Fermi energy. For the specific case of a Fermi energy $E_F = \pm 1$, the slope of the linear increase is about one.

In the derived Kubo formula, no disorder was included. But even if one work with ultra pure conductors, a small amount of impurity and weak scattering effects have to be included. Also the attached leads affects the conduction because of the arising interaction

between the leads and the probe. Both of these effects lead to a replacement of the parameter η by the imaginary part of a self energy Σ [9] [28]. This imaginary part can be related to the inverse life-time of a particle in the state $|m, k_y\rangle$ [9]

$$\eta = -\operatorname{Im}\Sigma(\varepsilon_m(k_y)) = -\frac{\hbar}{\tau(\varepsilon_m(k_y))}. \tag{100}$$

Thus, in the pure case with no disorder the life-time τ goes to infinity such that η goes to zero. But for finite life-time also η takes a finite value. This allows us to conclude that, simulate a specific amount of disorder, is equivalent to tune the parameter η to the corresponding value.

To be able to compare the later results, with the measured oscillation in [5], one has to estimate η for the specific length scales summarized in table 1. Due to the large anisotropy $\kappa = 0.001$, the bands are nearly flat. This allows us to estimate the Fermi velocity by the group velocity. The bands are then nearly degenerated in energy, such that elastic scattering is able to change the states of a specific band over the whole momentum range. Therefore one can roughly estimate the life-time by the scattering time, such that it can be calculated by eq.(3),

$$\tau_m = \frac{l_y}{\bar{\nu}_m}. \tag{101}$$

For the mean free path in y-direction we assume that it is in a range of one third the crystallographic unit cell, in a way we say that the electron, travelling in y-direction, scatters in every conducting layer. Note: the length of the crystallographic unit cell was used in units of the lattice constant. In the used Hofstadter model eq.(40), each tunnelling matrix element is modulated by a phase $e^{i2\pi(\phi/(L-1))j}$. Summing over all matrix elements yields the series

$$A(\phi) = \sum_{j=0}^{L-1} e^{i2\pi(\phi/(L-1))j} = \frac{1 - e^{i2\pi\phi}}{e^{-i2\pi(\phi/(L-1))} - 1}. \tag{102}$$

Then the group velocity is approximated by

$$\begin{aligned} \nu_m &\sim \frac{t_y}{(L-1)} \operatorname{Im} A(\phi) \sim t_y \frac{1 - \cos(2\pi\phi)}{2\pi\phi} \\ \bar{\nu}_m &= \frac{t_y}{\phi_{max}} \int_0^{\phi_{max}} \frac{1 - \cos(2\pi\phi)}{2\pi\phi} d\phi. \end{aligned} \tag{103}$$

For the maximal flux range $\phi/\phi_0 \in [0, 20]$, calculated under consideration of the maximal field strength $14T$ and the area S reported in [5], the parameter η should be between 0.0002 and 0.0004. Note: we have here assumed that $\kappa = 0.001 \pm 0.0001$ to include possible measurement errors.

With the connection of the parameter η to the inverse life-time τ, we are able to

give an explanation for the increase of the inter-band conductivity with increasing η. Incoherent scattering processes like the electron-phonon scattering broadens the energy levels. Due the this broadening the level separation is reduced, what enhances the inter-band hopping probability. This broadening can be seen indirectly in the model as the range of bands, that gave non zero contribution, is enlarged.

The question is, why to include inter-band contribution when dealing with coherent transport. **Increasing L, the level separation becomes smaller than the level broadening from such incoherent processes**. This motivates the inclusion of inter-band contributions when study system, that width is of order $L \sim 10^4$.

6. Equivalence between Kubo and Landauer Buettiker

Working with mesoscopic systems, the natural way to study transport phenomena is due to the Landauer theory of electronic transport. In the case of DC current one can proof the equivalence between the Kubo formula and Landauer Buettiker. We will do this in analogy to Fisher and Lee (1981) [31].

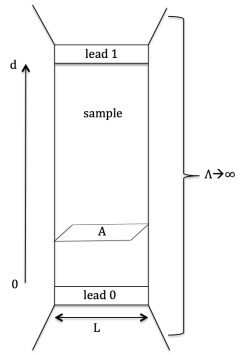

Figure 19: Schematic picture of the mesoscopic system. The sample is of size L × d. A defines the area of the cross section. Working with its approximation by a two dimensional lattice, the leads are attached in y-direction and the finite width is chosen in x-direction.

Starting with the expression of the conductivity in eq.(83) and rewrite it as its associated conductance in the zero temperature limit, one get

$$G(\omega) = \frac{\pi\hbar}{\omega d^2} \sum_{n,m} |\langle n|J_y|m\rangle|^2 \delta(\hbar\omega + \varepsilon_n - \varepsilon_m). \tag{104}$$

The system we study is of size $L \times d$, with crossection A Fig.19. We take its approximation by a two dimensional lattice model of size $L \times d$. Attaching leads in y-direction makes the system infinite in this direction. The disordered region of interest is then embed in an infinite system with no disorder. We will work in real space representation where periodic boundary conditions are assumed in transverse direction x. Even if the in-plane dimension of the systems is small, because we are interested in bulk coherent transport and neglect boundary effects, this assumption is justified. Also we just want to to show the equivalence for longitudinal transport, not for transversal one. Then the conductance in eq.(104) becomes

$$G(\omega) = \frac{\pi\hbar}{\omega d^2} \sum_{n,m} |\int_0^d dz \underbrace{\langle n|J_y(y)|m\rangle}_{J_{nm}(y)}|^2 \delta(\hbar\omega + \varepsilon_n - \varepsilon_m). \tag{105}$$

The real space representation of the states is given by the wave function $\Psi_n(\vec{r}) = \langle \vec{r}|n\rangle$,

$\Psi_m(\vec{r}) = \langle \vec{r}|m\rangle$ where $\vec{r} = (x, y)$. Then the current operator can be written as

$$\begin{aligned} J_{nm}(y) &= \frac{e}{i2m\hbar}\int dx \left(\langle n|\partial_y^\dagger|\vec{r}\rangle\langle\vec{r}|m\rangle - \langle n|\vec{r}\rangle\langle\vec{r}|\partial_y|m\rangle\right) \\ &= \frac{e}{i2m\hbar}\int dx \left(\partial_y\Psi_n^*(\vec{r})\Psi_m(\vec{r}) - \Psi_n^*(\vec{r})\partial_y\Psi_m(\vec{r})\right). \end{aligned} \tag{106}$$

Current conservation implies that for a DC current, the current operator is independent of y

$$J_{nm}(y_0) - J_{nm}(y_1) = i\omega\int_{y_0}^{y_1} dy\int dx\Psi_n^*(\vec{r})\Psi_m(\vec{r}) \xrightarrow{\omega\to 0} 0. \tag{107}$$

Because of that, the integral over y can be done trivially and J_{nm} can be evaluated outside the disordered region. Evaluating in the leads, the eigenstates are simple given by combinations of plane waves.

The conductance can be written in terms of single particle Green's function defined by $G^\pm(\varepsilon + i\eta) = [\varepsilon \pm i\eta - H_0]^{-1}$. There the $\pm$ sings denote the retarded and avanced Green's function. In real space representation the Green's function is given by the matrix element between two scattering channels i and j

$$G_{i.j}^\pm(y, y') = \frac{1}{L}\int dx\int dx' e^{-ip_j x}e^{ip_i x'}\langle\vec{r}_j|G^\pm|\vec{r'}_i\rangle, \tag{108}$$

where y' is in lead 0 and y in lead 1.
Note: each plane wave corresponds to a scattering channel i, j, where $p_{i,j}$ is the transverse momenta.
Eq.(105) can be written as

$$G(\omega) = \frac{\pi\hbar}{\omega d^2}\int d\varepsilon\sum_{n,m}\left|\int_0^d dy J_{nm}(y)\right|^2\delta(\varepsilon + \hbar\omega - \varepsilon_m)\delta(\varepsilon - \varepsilon_n). \tag{109}$$

We rewrite the delta function in terms of Green functions

$$\delta(\varepsilon - H_0) = \frac{-1}{2\pi i}(G^+ - G^-), \tag{110}$$

with $G^\pm$ in real space representation.
Taking the DC limit, the energy integration turns to a delta-distribution.

$$\int d\varepsilon(\varepsilon + \hbar\omega - \varepsilon_m)\delta(\varepsilon - \varepsilon_n) \to \int d\varepsilon\delta(\varepsilon - \varepsilon_m)\delta(\varepsilon - \varepsilon_n) = \delta(\varepsilon_n - \varepsilon_m). \tag{111}$$

Thus the summation over states is replaced by a trace over the matrix representation of the Green functions

$$\sum_{n,m}\delta(\varepsilon_n - \varepsilon_m) = \frac{-1}{(2\pi)^2}Tr\left\{\left(G^+ - G^-\right)\left(\tilde{G}^+ - \tilde{G}^-\right)\right\}, \tag{112}$$

where $\tilde{G}_{ij}^\pm(y, y') = G_{ij}^\pm(y', y)$. By the use of this, the DC limit of eq.(109) is given by

$$G(\omega=0)=\frac{-\pi\hbar}{(2\pi)^2}Tr\left\{|J(y,y')|^2\left(G^+-G^-\right)\left(\tilde{G}^+-\tilde{G}^-\right)\right\}, \tag{113}$$

with $J(y,y')$ being the current matrix, whose matrix elements can be defined similar to eq.(108). Note: if the momentum operator, in real space representation, acting on a prime state we write $\partial_{y'}$. Such that the DC conductance can be written in a simpler way concerning calculations.

$$\begin{aligned}G=\frac{-e^2\hbar}{4m^2}\frac{\pi}{(2\pi)^2}Tr\Big\{&\partial_{y'}\partial_y(G^+-G^-)(\tilde{G}^+-\tilde{G}^-)+(G^+-G^-)\partial_y\partial_{y'}(\tilde{G}^+-\tilde{G}^-)\\&-\partial_y(G^+-G^-)\partial_{y'}(\tilde{G}^+-\tilde{G}^-)-\partial_{y'}(G^+-G^-)\partial_y(\tilde{G}^+-\tilde{G}^-)\Big\}\end{aligned} \tag{114}$$

The Green functions in real space representation consists of incoming and outgoing plane waves in y-direction. As example $G^+_{i,j}$ consists of outgoing waves only, so that $G^+_{i,j}(y,y')$ is proportional to $\exp(-ik_jy')$ and $\exp(ik_iy)$. Then the $\partial_{y,y'}$ acting on it has the following effect:

$$\begin{aligned}\partial_y(G^+-G^-)&=(G^++G^-)\\\partial_{y'}(G^+-G^-)&=(-G^+-G^-)\\\partial_y(\tilde{G}^+-\tilde{G}^-)&=(-\tilde{G}^+-\tilde{G}^-)\\\partial_{y'}(\tilde{G}^+-\tilde{G}^-)&=(\tilde{G}^++\tilde{G}^-)\end{aligned} \tag{115}$$

leading to the expression for the conductance

$$G=\frac{e^2}{4\pi\hbar}\sum_{ij}\left(|G^+_{ij}(y,y')|^2+|G^+_{ij}(y',y)|^2\right)\nu_i\nu_j, \tag{116}$$

with the velocity $\nu_{i/j}=\dfrac{k_{i/j}}{m}$ in channel i/j. To find a relation to the scattering matrix one has to relate the Green function to the transmission matrix. D.Fisher and A.Lee found such a relation [31]. By the use of scattering theory they calculated

$$t^0_{ij}=-i\nu_iG^+_{ij}(y,y')\exp(-i(k_iy-k_jy')), \tag{117}$$

for the transmission amplitude of waves transmitted from lead 0. A similar expression is found for the transmission t^1. Normalizing the channels to carry one flux quantum in y-direction and also normalize the wave function in this manner, leads for the conductance to the well known expression

$$G=\frac{e^2}{2h}\sum_{ji}\left(|t^0_{ji}|^2+|t^1_{ji}|^2\right))=\frac{e^2}{h}Tr\left\{t^\dagger t\right\}. \tag{118}$$

This expression is equivalent to eq.(56) for the case of zero temperature and without the factor two from spin degeneracy. Note: the equivalence hold also for finite temperature, when assuming small bias voltage as in chapter 4.1

7. Kwant

Kwant is a python tool for simulating quantum transport, calculating band structures and contains an integration tool kit. We will use it to calculate the conductivity in the Landauer formalism. Showing the different steps from the definition of the system in Kwant up to the explicit calculations of the conductivity, should give the reader an insight of how this software works. The explanation of the different functions and ways of implementation is based on the official Kwant documentation see [21].

7.1. Defining a system with Kwant

In general one start with the problem of a Hamiltonian, for which different properties have to be calculated. To use Kwant one has to discretize the Hamiltonian. Let's take for an example the Hamiltonian of a two dimensional quantum wire, that is given by the Schroedinger equation,

$$H = \frac{-\hbar}{2m}\left(\partial_x^2 + \partial_y^2\right) + V(x), \tag{119}$$

with a hard-wall confinement $V(x)$ in x-direction. This continuous model has to be discretized on the sites of a square lattice, with lattice constant a. Thus each lattice coordinate (i, j) is related to the real-space coordinate by $(x, y) = (ai, aj)$, therefore the discretized positional states are:

$$|i, j\rangle \equiv |ai, aj\rangle = |x, y\rangle. \tag{120}$$

Taking the limit $a \to 0$ to express the second-order differential operator

$$\partial_x^2 = \frac{1}{a^2}\sum_{i,j}\left(|i+1, j\rangle\langle i, j| + |i, j\rangle\langle i+1, j| - 2|i, j\rangle\langle i, j|\right). \tag{121}$$

By using these expression the discretized Hamiltonian reads

$$\begin{aligned} H = &\sum_{i,j}\left[\left(V(ai, aj) + 4t\right)|i, j\rangle\langle i, j|\right. \\ &\left. - t\left(|i+1\rangle\langle i, j| + |i, j\rangle\langle i+1, j| + |i, j+1\rangle\langle i, j| + |i, j\rangle\langle i, j+1|\right)\right], \end{aligned} \tag{122}$$

with hopping amplitude $t = \frac{\hbar^2}{2ma^2}$.

The question is now, how to implement this in Kwant?
To define a system in a convenient way one makes use of the *Builder* type. This object defines a tight binding system on a graph, where the nodes of the graph are *Site* instances. The hoppings (visualized as edges) are pairs of sites (tupel). Each node and edge has a value associated with it. The values associated with nodes are interpreted as on-site Hamiltonians, the ones associated with edges as hopping integrals. An example of a simple square lattice, related to the discretized Hamiltonian eq.(122) is given in Listing 1.

```
def make_system(a=1, t=1.0, w=15, d=30):
  lat = kwant.lattice.square(a)
  syst = kwant.Builder()

  syst[(lat(x,y) for x in range(w) for y in range(d))] = 4*t
  syst[lat.neighbors()] = -t

  lead = kwant.Builder(kwant.TranslationalSymmetry((0,-a)))
  lead[(lat(j,0) for j in range(w))] = 4*t
  lead[lat.neighbors()] = -t
  syst.attach_lead(lead)
  syst.attach_lead(lead.reversed())

  return syst

def main():
  syst = make_system()
  syst = syst.finalized()
  kwant.plot(syst)

if __name__=='__main__':
  main()
```

Listing 1: Kwant code for the implementation of a simple square lattice.

The function *make system* defines a square lattice of size $w \times d$ with lattice constant a, where two leads are attached. After using the *Builder()* function, one can start to give certain values to the nodes and sites. This is done in a way giving a on-site potential to the lattice nodes and by defining a hopping value for next-nearest neighbour hopping. Note that the function *neighbors*, which defines the hopping, automatically takes care of translational symmetry. If one would stop now, the defined system remains as a closed system. Attaching leads makes it infinite in the lead direction. Leads can also be defined using the *Builder* function in the case where the system has translational symmetry. The symmetry can be given as an additional argument in the *Builder* function. The real-space vector $(0, -a)$, that defines the translational symmetry, must point away from the scattering region into the leads. It is enough to add one unit cell of the leads as well as the hopping inside one unit cell and to the next unit cell of the lead. At this state, just a builder type object is created. To use it for calculations one has to finalize the system, which creates a so-called low level system, that can be used by the functions in the solver package of Kwant. The command *kwant.plot* gives a graphical representation of the lattice Fig.20

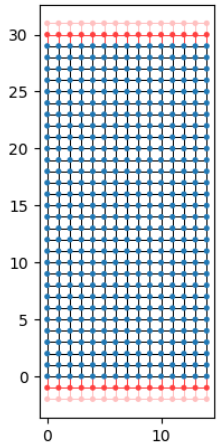

Figure 20: Square lattice w=15 and d=30, with lattice constant a=1.

The system we want to study includes anisotropic hopping. It is therefore usefully, to take the hopping strength in y-direction as a variable κ. The same way differences between bulk and edge hopping can be handled, introducing the parameters $b = t^y_{edge}/t^y_{bulk}$. This is done be replacing the simple hopping parameter $-t$, by a specific hopping function.

```
1  def hopping(site_i, site_j, kappa, b):
2    xi, yi = site_i.pos
3    xj, yj = site_j.pos
4    if xi == xj:
5      if xi == 0 or xi == w-1:
6        return -b*kappa*t
7      else:
8        return -kappa*t
9    else:
10     return -t
```

Listing 2: Defnition of a function that handels different hopping constraints.

The function in Listing 2 takes as input variables, beside problem specific parameters, two sites. By *.pos* the real space position of a site is extracted, allowing to give site dependent conditions on the hopping. Note: also if we define a hopping function, the reversal hopping is included by the transversal symmetry of the function *neighbors*.

Including a magnetic field perpendicular to the plane leads to a phase dependent hopping (see chapter 2). The hopping phase will be defined in the Landau gauge $\vec{A} = (0, Bx, 0)^T$. The induced hopping phase is given by (see Appendix C)

$$\exp\left(\int_{\vec{x}_i}^{\vec{x}_j} \vec{A}(\vec{s})d\vec{s}\right) = \exp\left(-\frac{i}{2}\Phi(x_i + x_j)(y_i - y_j)\right), \tag{123}$$

where the indices i, j define the site position and *phi* the flux per plaquette in units of ϕ_0. Including this phase factor in the hopping function is done in Listing 3.

```
1  def hopping(site_i, site_j, kappa, b, phi):
2    xi, yi = site_i.pos
3    xj, yj = site_j.pos
4    if xi == xj:
5      if xi == 0 or xi == w-1:
6        return -b*kappa*t*exp(-0.5j*phi*(xi + xj)*(yi - yj))
7      else:
8        return -kappa*t*exp(-0.5j*phi*(xi + xj)*(yi - yj))
9    else:
10     return -t
```

Listing 3: Hopping function with included phase factor, that arises due to an additional magnetic field.

It remains to include some scattering effects. This effects have only to be included in the scattering region and not in the leads, see chapter 4. First including impurities as random on-site potential.

A random on-site potential is defined by $V_{dis} = \sum_i U_i |\mathbf{x}_i\rangle\langle\mathbf{x}_i|$, with U_i choosen randomly from a uniform distribution $[-U_0/2, U_0/2]$.

```
1  def onsite(site, U0, salt):
2    return U0 * (uniform(repr(site), repr(salt)) - 0.5) + 4 * t
```

Listing 4: Definition of a random on-site potential.

The function *uniform...*, in Listing 4, takes both of its arguments *input* and *salt*, combines them in a stream of bytes and applies the MD5 message-digest algorithm on it. The output of this algorithm is then taken and turned into a floating point number in range $[0, 1)$, that is returned.

In a second step we want to summarize the effects of further scattering at impurities, of weak electron-electron or electron-phonon scattering. This is done in adding an additional hopping term to the y-hopping, that is randomly chosen from a set bounded by the maximal additional hopping contributions, shown in Listing 5.

```
1  delta = random.choice(dtset)
2  -kappa*(t + delta) *exp(-0.5j*phi*(xi + xj)*(yi - yj))
```

Listing 5: Including random hopping in Kwant.

There the function *random.choice(dtset)* does the job of choosing a random value of the set *dtset*. Note: the effect of electron-electron scattering or electron-phonon scattering has to be very weak because otherwise phase coherence would be lost. However, since we

are dealing with finite temperature, at least the effect of reducing the hopping amplitude has to be taken into account.

7.2. Evaluation of the band structure

It is important to evaluate the band structure again and compare it with the one evaluated in chapter 2, to prevent us from doing some mistakes in the implementation of the system in Kwant.

Kwant has the benefit, that system related properties, like the band dispersion, can be directly read out from the leads using *kwant.physics.Bands*. This function *.physics* gives access to all physical properties contained in the lead.

```
1 bands = kwant.physics.Bands(syst.leads[1],
2           params=dict(phi=phi, kappa=kappa, b=b))
```

Listing 6: Calculation of the band structure with the Kwant physics tool.

In Listing 6, the parameters are included as a dictionary in the function *Bands*. Note: the choice of the lead does not play a role, because of the symmetry.

In the band calculations Fig.21, the on-site potential was chosen as zero, instead of $4t$ to get a spectrum that is symmetric around zero for better comparison with the plots in chapter 2. Changing the on-site potential, at every place by the same value, only shifts the spectrum and has no further effect.

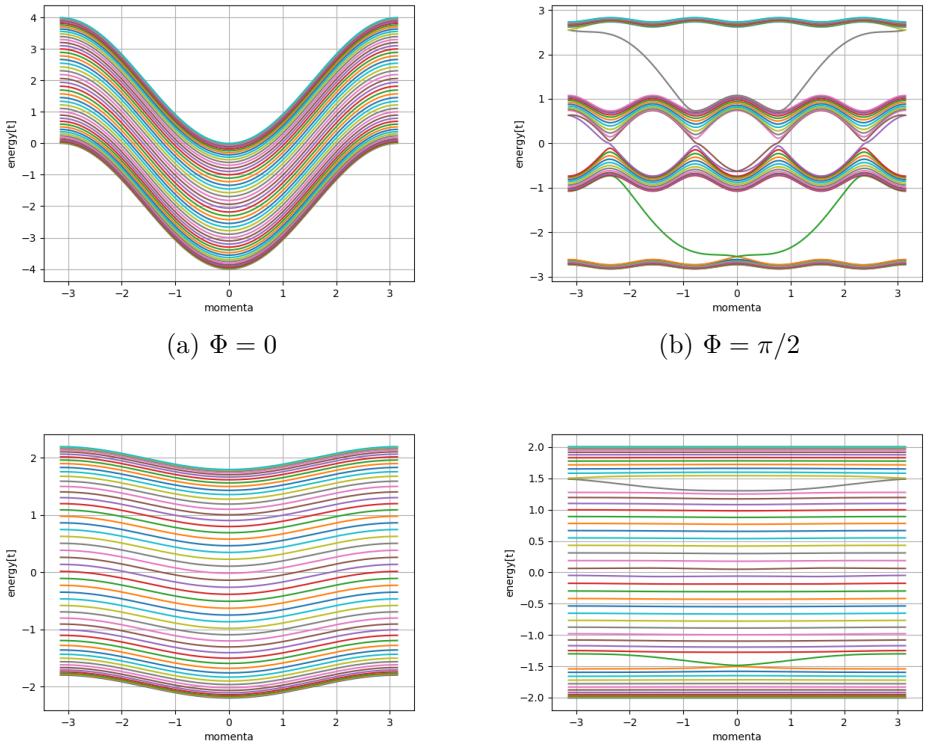

(a) $\Phi = 0$ (b) $\Phi = \pi/2$

(c) $\Phi = 0$ (d) $\Phi = \pi/2$

Figure 21: Band structure for isotropic system **a,b** and anisotropic system **c,d**, at different flux per plaquette Φ.

The calculation of the spectrum as a function of the magnetic flux, can be done in two ways. One can use the information contained in the leads as in the calculation of the band structure and evaluate it for each flux value. Another strategy is to create an Hamiltonian matrix out of the system and using its energy eigenvalues Listing 7.

```
1 def plot_spectrum(syst, fluxes, hop):
2   energies = []
3   count = 0
4   for phi in fluxes:
5     ham_mat = syst.hamiltonian_submatrix(params=
6               dict(phi=phi, hop=hop), sparse=True)
7     ev = np.real(np.sort(np.linalg.eigvals(ham_mat.todense())))
8     energies.append(ev)
9   return energies
```

Listing 7: Calculation of the spectrum as a function of magnetic flux per plaquette, using the Hamiltonian matrix of the lattice.

The function *syst.hamiltonian_submatrix* takes as input a finalized system and creates a hopping matrix out of it. Because we are dealing only with nearest neighbour hopping,

it makes sense to take the matrix as a sparse matrix. Then the eigenvalues can be calculated using the general numpy or scipy tools. There is one important point one has to take care off. The Hamiltonian matrix has dimension $(w * d \times w * d)$. Thus it takes the finite dimension of the scattering region also in y-direction. Working this way one has to chose the y-dimension large enough to get a comparable amount of points as momenta.

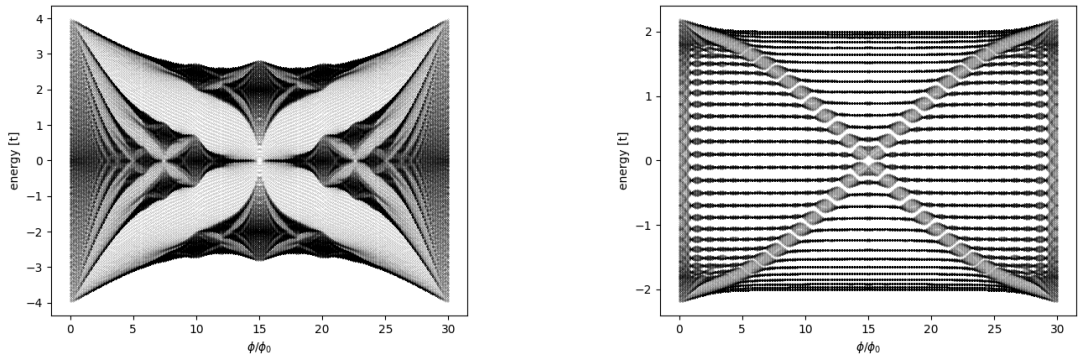

Figure 22: Energy spectrum for a system of size $L = 30$, as a function of magnetic flux. **Left**: isotropic hopping. **Right**: anisotropic hopping $\kappa = 0.1$.

The results in Fig.21,22 are equivalent to the one calculated in chapter 2. Because of this we can be sure that the implementation was done the right way.

7.3. Implementation of the Landauer formalism

Calculating the conductance in the Landauer formalism, the scattering matrix is needed. Kwant is able to directly calculate the scattering matrix for a given system. This can be done by using the tool *kwant.solvers.common.Smatrix*. As input parameters this function takes the system, energy and additional parameter given by a dictionary. The data stored in *Smatrix* is a scattering matrix with respect to the lead modes and these modes themselves. One gets access to the transmission from lead 0 into lead 1 by *SMatrix.transmision(0,1)*. A detailed description of how Kwant calculates the scattering matrix can be found in Appendix D. The conductance is then calculate in the Landauer-Buettiker formalism, derived in chapter 4.1

$$G(\varepsilon) = \frac{2e^2}{h} \int_{-\infty}^{+\infty} T(\varepsilon) \left(-\frac{\partial f}{\partial \varepsilon} \right) d\varepsilon, \tag{124}$$

with $T(\varepsilon) = \sum_n T_n(\varepsilon)$, where n is the number of channels.

The implementation is shown in Listing 8. To calculate the conductance eq.(124), for a specific input energy, one has to convolute the derivative of the Fermi distribution with the transmission function

$$\boxed{G(\varepsilon) = \frac{2e^2}{h} \int_{-\infty}^{+\infty} \left(-\frac{\partial f(\varepsilon')}{\partial \varepsilon'} \right) T(\varepsilon - \varepsilon') d\varepsilon'} \tag{125}$$

Integration over the full energy range takes some time. But because the derivative of the Fermi function is highly peaked around the Fermi energy, it is enough to integrate over $[\varepsilon_F - \text{few} \cdot k_B T, \varepsilon_F + \text{few} \cdot k_B T]$. To calculate the transmission between the two leads, one can use the solver class in Kwant *kwant.solvers.common*. In this class the function *Smatrix* calculates the scattering matrix and *Smatrix.transmission(0,1)* gives back the transmission, between lead 0 and lead 1. The integration is done by *numpy.trapez*, that approximates the integral by the Heun method.

```
def band_conductance(syst, temp, EF, energy):
  H = []
  erange = np.linspace(EF-5*temp, EF+5*temp, 300)
  for en in erange:
    flag = True
    while flag:
      try:
        H.append(fermideriv(en=en,Efermi=EF,temp=temp)
        *kwant.smatrix(syst,(energy-en)+EF,
        params=dict(phi=phi,hop=hop,var=var,U0=U0))
        .transmission(0,1))
        flag = False
      except:
        en += 0.000000000001
        H.append(fermideriv(en=en,Efermi=EF,temp=temp)
        *kwant.smatrix(syst,(energy-en)+EF,
        params=dict(phi=phi,hop=hop,var=var,U0=U0))
        .transmission(0,1))

   cond = np.trapz(H, erange)

   return cond
```

Listing 8: Calculation of the band conductance, using the transmission function implemented in Kwant.

The energy dependence of the S-matrix brings in some numerical instabilities for some specific energies. Source of the instabilities are singularities in the leads at specific energies, that means divergence of the lead modes. This problem is solved by isolating that energies and exchange them by slightly different energies, which is valid if the change in energy is much smaller then the difference between the isolated and the upcoming one. Note: adding *EF* in the argument of the *smatrix* function just shifts the whole values back in the right energy range.

Calculation of the conductance as a function of magnetic flux, works similar. Fixing one particular input energy and varying the flux argument. To get out the conductivity the conductance has just to be divided by the sample width w.

8. Results and Discussion

The following sections contains the results of conductivity calculations using the Kubo formula as well as the Landauer approach. If not explicitly study the effect of changing width, we fixed $L = 50$ to deal with a reasonable computation time. Note: increasing width goes always along with an increasing number of channels L. With respect to the band structure, L is the number of bands that order into q bands under the influence of a magnetic field. Thus whenever we talk about the bands built due to the magnetic field we denote it with q-bands. The mesoscopic systems we want to study have a width of order $L \sim 10^4$, thus one has to include scaling effects in the discussion. All fluxes are given in units of magnetic flux quanta $\phi_0 = h/e$ and the energies in units of the hopping amplitude t. The conductivity is given in units of e^2/h.

8.1. Results using Landauer theory

Conductivity without magnetic field

The behaviour of the conductivity in Fig.23 is in agreement with the one expected from the band structure effected by anisotropy. Increasing the anisotropy turns the conductivity maxima to the outer energy regions, where the maximal DOS is located. The overall decrease in conductivity with increasing anisotropy is based on the reduced curvature that results in a reduced group velocity. Reducing curvature, therefore the bandwidth, enhances the level separation. This of course turns out to get a bigger effect, the higher the level spacing, therefore the lower system dimension. Due to the level separation an oscillatory behaviour in conductivity results. The missing of oscillations with increasing temperature is due to the level broadening and thus reduced level separation. In eq.(56) this is reflected in the derivative of the Fermi function that gets smoother with increasing temperature.
Note: subfigure **d)** shows, for the case of higher temperature, a conductivity that is slightly higher then the value one would get by the average of the oscillation at lower temperature. This is a result of the low number of levels and vanishes for increasing L.

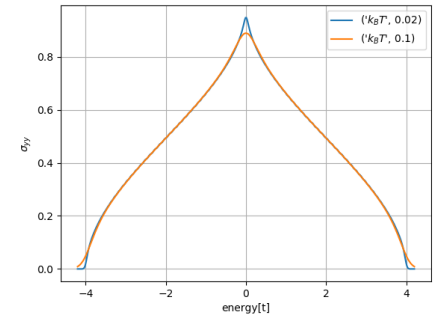

(a) $\kappa = 1$

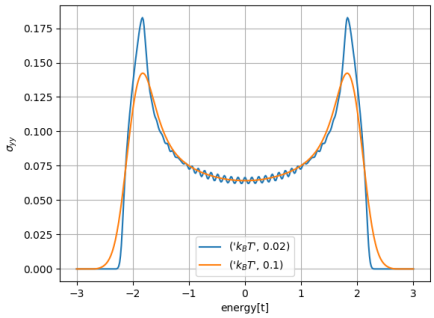

(b) $\kappa = 0.1$

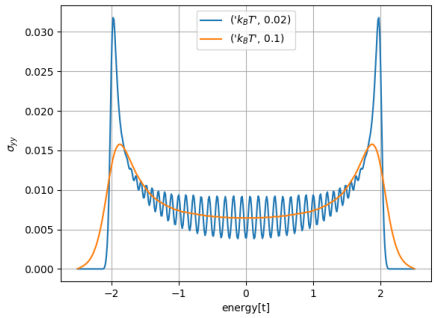

(c) $\kappa = 0.01$

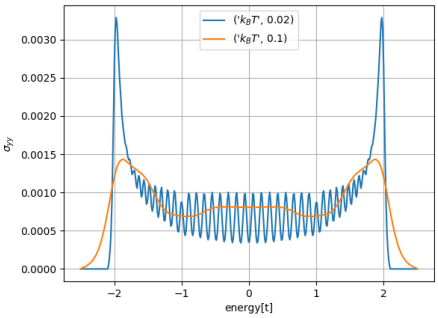

(d) $\kappa = 0.001$

Figure 23: Conductivity as a function of energy, calculated at different temperatures and different anisotropy κ.

Conductivity for fixed magnetic flux per plaquette

Fig.24,25 shows the conductivity as function of energy, for the case of different flux per plaquette. The peaks in the conductivity are equally placed in energy as the formation of the q-bands, that goes along with a maximal DOS. For increasing anisotropy it overcomes the effect of the magnetic field, thus as the DOS, it turns in an oscillating behaviour, strongly peaked at the energy edges. One can observe that with increasing flux per plaquette, the conductivity at its maximal peaks increases also. This is explained by the decrease of the number of bands q and thus the higher occupation of the remaining ones.

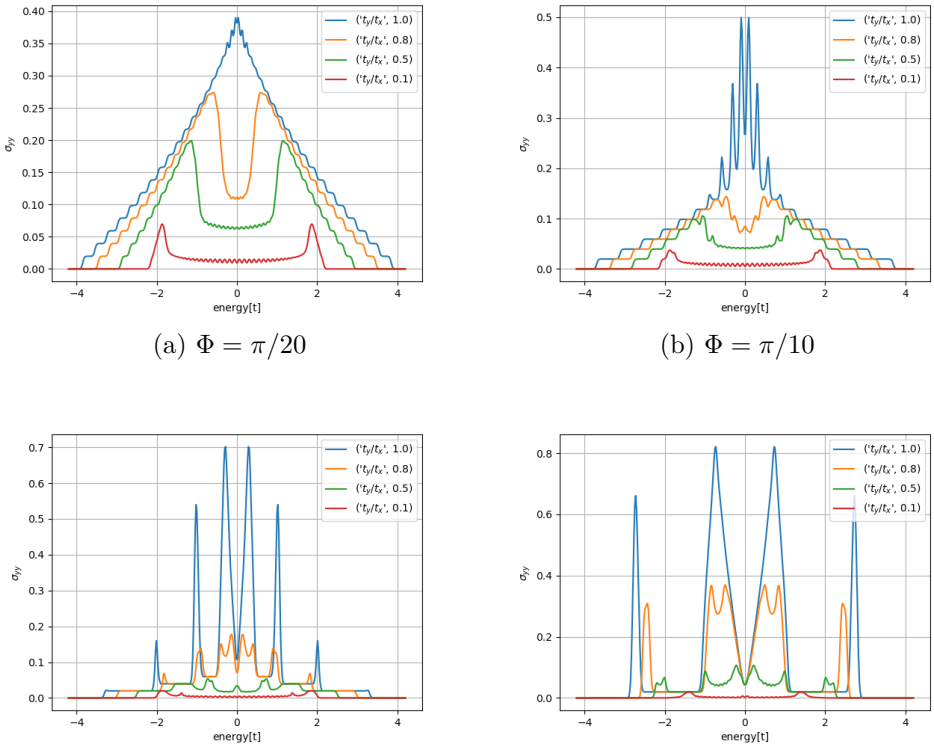

(a) $\Phi = \pi/20$ (b) $\Phi = \pi/10$

(c) $\Phi = \pi/4$ (d) $\Phi = \pi/2$

Figure 24: Conductivity as a function of energy, calculated at a temperature of $k_B T = 0.02$ and different anisotropy κ. The subfigures **a,b,c,d** shows the cases of different flux per plaquette Φ. The number of bands q, for a flux per plaquette given in subfigure **c)**, seems to disagree with the number of observed peaks. This is due to small contribution of the outer bands such that they are not visible.

From Fig.25 it is seen that for strong anisotropy, the choose of the Fermi energy has an enormous impact on the conductivity. A Fermi energy placed between bands corresponds to a minimum in conductivity. But for a mesoscopic system, that is in an order of $L \sim 10^4$, those gaps would nearly vanish and the spectrum gets close to a continuous one. Therefore choosing the Fermi energy in a gap does not describe the physics in the right way. In the calculation of the conductivity as a function of magnetic flux a Fermi energy of $E_F = -1$ was chosen.

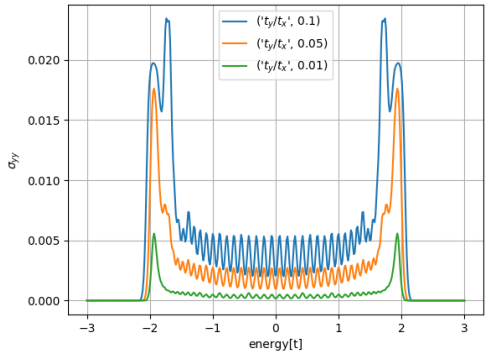

Figure 25: Conductivity as a function of energy, calculated at a temperature of $k_BT = 0.02$ and different anisotropy κ. A flux of $\Phi = \pi/6$ per plaquette was chosen.

Conductivity as function of magnetic flux

Fig.26 shows the behaviour of the conductivity as a function of the total flux ϕ/ϕ_0. The magnetic field leads to an oscillation in conductivity, that decreases with higher flux values. For small system size $L = 50$ the oscillation is wired for small anisotropy and becomes a smooth periodic oscillation with increasing anisotropy **b),c)**. With increasing system size, due to the reduced level spacing, the oscillation gets smooth also for smaller anisotropy **d)**. A further increase of anisotropy just lowers the conductivity in general, but remains the periodic structure with equivalent periodicity. We will discuss the reason for the observed periodic oscillation, after comparing it with the results using the Kubo formalism.

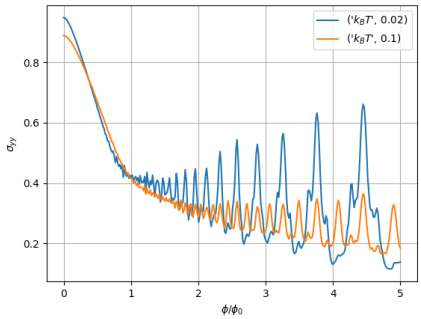

(a) $\kappa = 1$

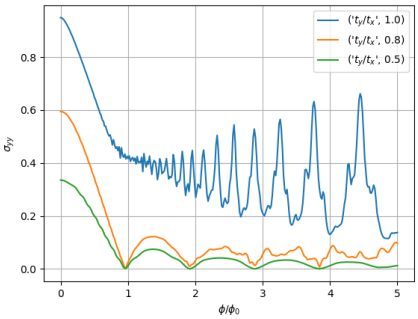

(b) $k_BT = 0.02$

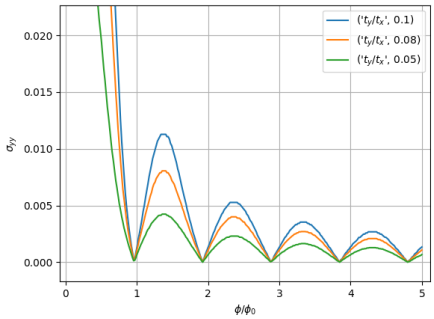

(c) $k_BT = 0.02$

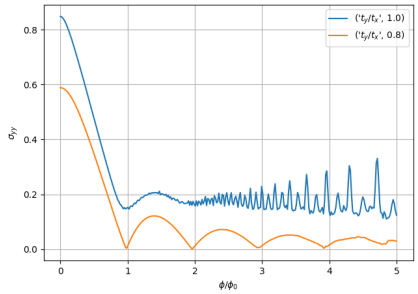

(d) $k_BT = 0.02$, $L = 150$

Figure 26: Conductivity as a function of magnetic flux in the case of **a)**: isotropic hopping and different temperatures; **b,c)**: different anisotropy at temperature $k_BT = 0.02$; **d)**: increased system size $L = 150$, $k_BT = 0.02$ and different anisotropy.

The subfigures in Fig.27 shows the effect of increasing channel number L on the conductivity, in the anisotropic case. In the left subfigure it is visible that, the larger L, the closer the minimum comes to the integer flux values. Therefore one can conclude that taking the limit $L \to \infty$, the minima will be placed at integer flux values. The right subfigure reveals a convergence of the conductivity with increasing L.

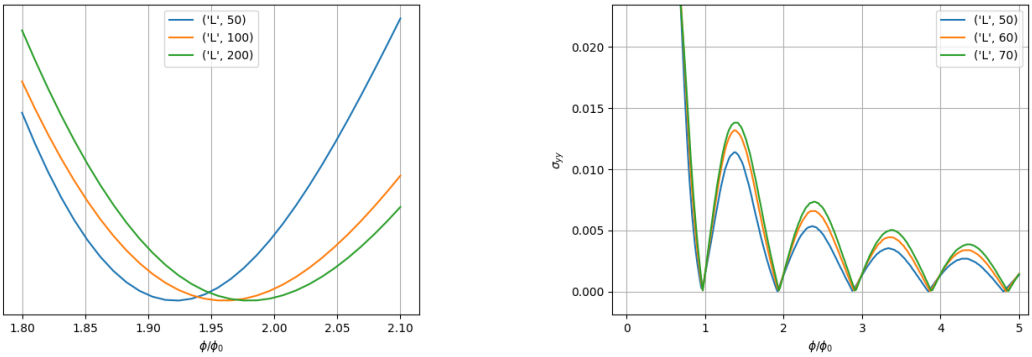

Figure 27: Conductivity at an anisotropy of $\kappa = 0.1$, for increasing width; **Left**: around a minimum. **Right**: full behaviour.

Fig.28 reveals the effect of added disorder. In the left subfigure a random on-site potential U_0 was added with different potential strength. Increasing potential strength lowers the conductivity, what is expected form a physical perspective. If the potential overcomes the value of the hopping amplitude, the conductivity rise down to zero very fast, for larger magnetic flux. For the case of an additional hopping disorder, shown in the left subfigure, the conductivity also decreases with increasing disorder strength, but the structure is getting more jagged than in the case of a random on-site potential. However, hopping disorder lowers the conductivity the same amount for all flux values. This is simply explained by the fact, that the disorder term δt, is also affected by the phase factor.

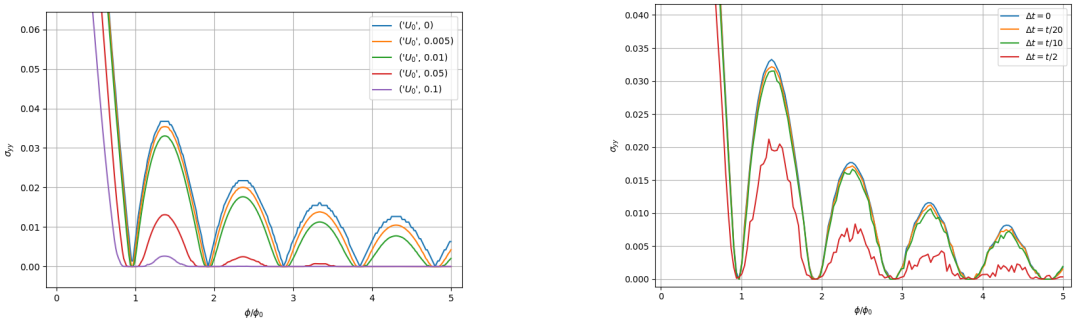

Figure 28: Conductivity as a function of total flux. **Left**: $\kappa = 0.01$, $k_B T = 0.02$, at different potential U_0; **Right**: $\kappa = 0.01$, at different hopping disorder δt and fixed potential $U_0 = 0.01$. The strength of the hopping disorder Δt is given with respect to the hopping amplitude t.

8.2. Results using Kubo formalism

As described in section 5.3, scattering effects enters the Kubo formula due to a finite value of η. Because of this parameter, the explicit size of the conductivity is hard to compare with the one calculated within the Landauer approach. However, this is just an internal scaling problem, thus the behaviour can be well compared. For the following computation the parameter was chosen $\eta = 0.05$. This we will show, satisfies the parameter range it has to be, for the calculations of the system described in [5]. In the calculations of the conductivity as a function of magnetic flux a Fermi energy of $E_F = -1$ was chosen, like in the Landauer case.

Intra-band conductivity

Conductivity without magnetic field

The results of the intra-band conductivity Fig.29 are in good agreement with the results from the Landauer approach. Even at strong anisotropy $\kappa = 0.001$, for the high temperature case, it shows the expected behaviour of averaging out the oscillation.
Note: No inter-band contribution is observed in the case of zero flux.

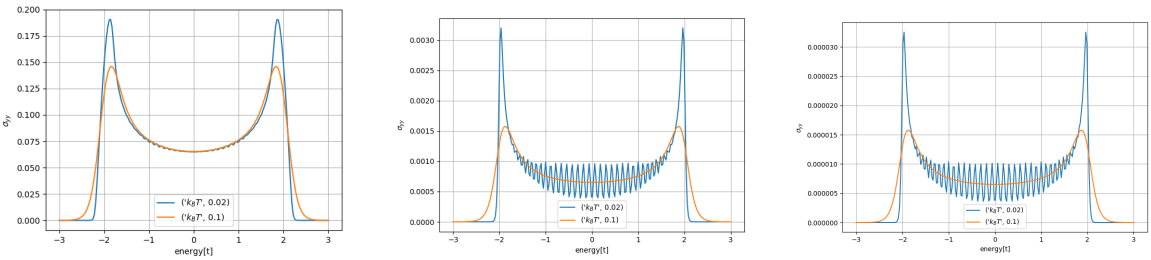

Figure 29: Intra-band conductivity as a function of energy at different temperatures, without magnetic field. The three subfigures show the case of different anisotropy. **Left**: $\kappa = 0.1$; **Middle**: $\kappa = 0.01$; **Right**:$\kappa = 0.001$.

Conductivity for fixed magnetic flux per plaquette

Fig.30 contains the intra-band conductivity for different anisotropy, at specific flux per plaquette, as a function of energy. Comparing the results, with the ones calculated by using the Landauer formula, shows some differences. Even if it is most of the time similar, thus strongly peaked at the q-bands, which contain a maximal DOS, there are some peaks less in the Kubo results. This can be well observed in subfigure **b)**, the case of $\Phi = \pi/4$. Even if the outer bands would give a much smaller contribution they should be observable. The absence of those peaks is due to the fact, that they are hidden by the contributions of the edge states. The edge states contain a much larger curvature then the other bands, what results in a large contribution compared to the contribution from the outer bands. In the case of a small width $L = 50$, those contributions dominate.

Increasing L, the DOS in the bands rises and overcomes the edge state contribution, such that they can be neglected and the conductivity between the bands is minimized. This is shown in subfigure **d)**, for energies in a range ± 1.2 to ± 2 in the case of $\Phi = \pi/2$.

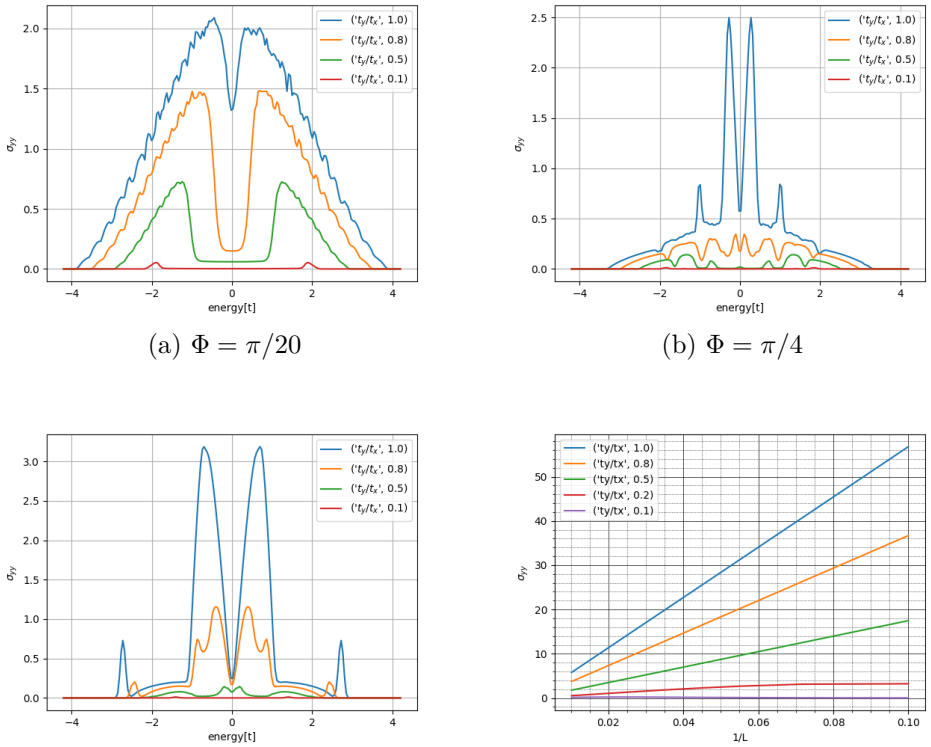

(a) $\Phi = \pi/20$ (b) $\Phi = \pi/4$

(c) $\Phi = \pi/2$ (d) $\Phi = \pi/2$

Figure 30: Intra-band conductivity as a function of energy, at different anisotropy. Subfigures **a,b,c)** show the case for different flux per plaquette Φ. Subfigure **d)** shows the conductivity at a specific energy of 1.5 and flux per plaquette $\Phi = \pi/2$, as a function of the inverse width.

Inter-band conductivity

For an applied magnetic field, the inter-band contribution turns out to be non-zero. Without magnetic field, the level separation is to large such that the hopping probability between different channels turns to zero. The magnetic field forms the q-bands consisting of a sum of narrow placed bands, whose separation is smaller than the level broadening, that would be induced by incoherent scattering processes. Because of that, the inter-band hooping will give a non-zero contribution to the conductivity. Fig.31 shows the behaviour of the inter-band conductivity for different anisotropy at specific flux per plaquette. The conductivity is peaked similar to the DOS. The bulk Dirac points, at an energy $E_F = 0$, give a large contribution due to the degeneracy of the states. Increasing the anisotropy, the Dirac points vanishes and the conductivity is maximally peaked in the outer energy

range, where the maximum in DOS is located.

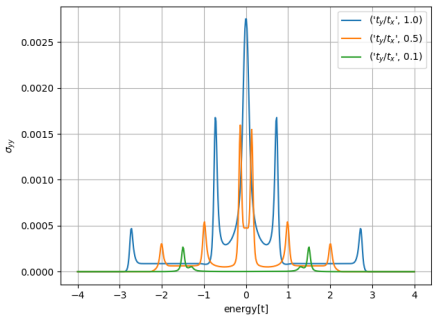

(a) $\Phi = \pi/2$

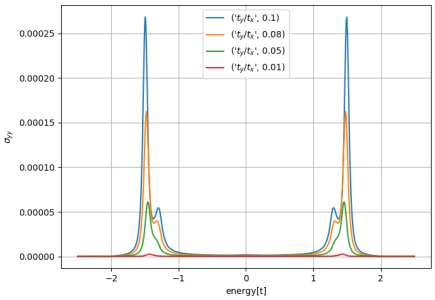

(b) $\Phi = \pi/2$

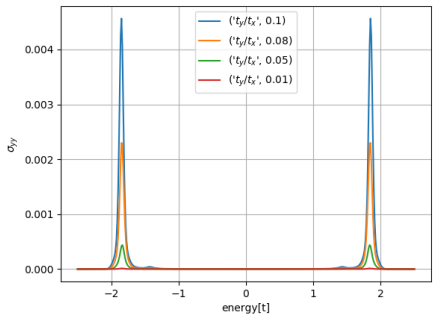

(c) $\Phi = \pi/4$

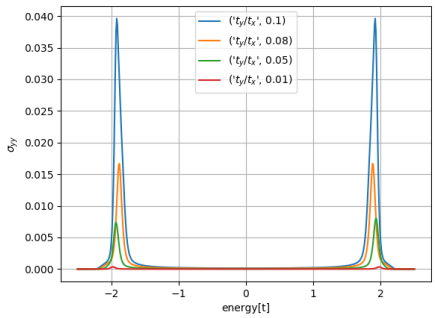

(d) $\Phi = \pi/35$

Figure 31: Inter-band conductivity as a function of energy, at a temperature of $k_B T = 0.02$, in the case of different anisotropy. The flux per plaquette is given by **a,b)**: $\Phi = \pi/2$; **c)**: $\Phi = \pi/4$; **d)**: $\Phi = \pi/35$.

Intra-band conductivity

Conductivity as function of magnetic flux

Fig.32 shows a similar behaviour as using the Landauer approach. The same way, an increasing number of channels reveals the smooth periodic behaviour also at smaller anisotropy. At this point, one has to give an explanation of the observed oscillatory behaviour. Consider the expression of the group velocity given in eq.(102). This function of ϕ reveals minima at integer flux values. This minima are reflected in the band structure, as the bands gets flat at integer flux values Fig.33. The flat bands have zero curvature, what is equivalent to a vanishing group velocity and thus to a vanishing conductivity. The behaviour of reduced conductivity, with increasing flux, can be explained by the increase of the denominator $2\pi\phi$ in eq.(102).

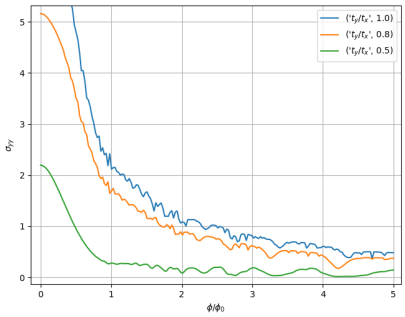

(a) $k_BT = 0.02$

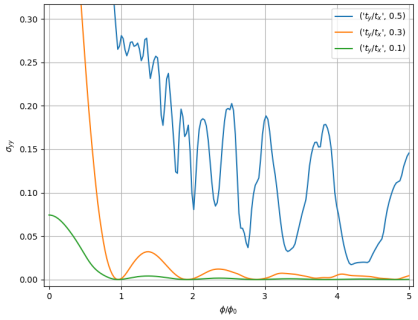

(b) $k_BT = 0.02$

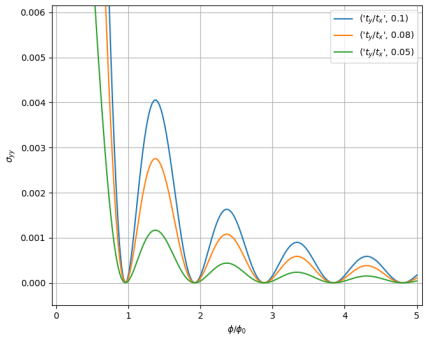

(c) $k_BT = 0.02$

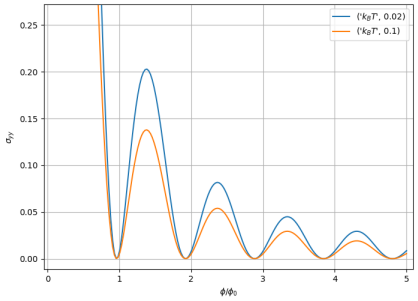

(d) $\kappa = 0.1$

Figure 32: Intra-band conductivity as a function of total flux. **a,b,c)**: at specific temperature $k_BT = 0.02$; **d)**: at specific anisotropy $\kappa = 0.1$.

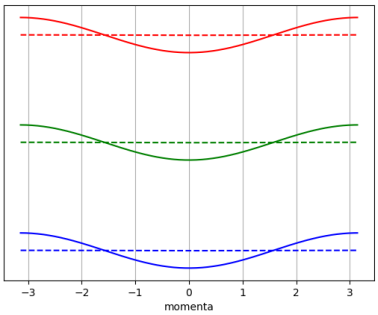

Figure 33: Energy spectrum at different flux values: $\phi = 0$ solid, $\phi = 1$ dashed. It reveals a vanishing bandwidth at integer flux values

Here we want to give a remark. In the case of the Landauer conductivity a convergence tendency was observed for increasing width. We also observed this in the case of the intra-band conductivity. The width at which it converges depends slightly on the anisotropy.

For $\kappa = 0.1$ it converges at $L = 120$ and for an anisotropy of $\kappa = 0.001$, at a value of $L = 160$. This is because for low values of L, the effect of an additional channel together with the reduced level spacing overcomes the normalization. At a certain value the additional contribution due to the reduction of the level spacing is irrelevant and the conductivity converges. However, there is a big surprise when comparing the results in [5] to the results reported here, for the behaviour of the intra-band conductivity in the case of increasing width. They reported a decrease in conductivity for increasing width. This behaviour can only be seen if one is choosing $E_F = 0$ and the width as $L = 31, 41, 51....$ In Fig.(34) we have shown that also for $E_F = 0$ choosing L differently, even or odd, in the limit of large L, they converge to the same value. Thus in the limit of large L there is no difference between this choices.

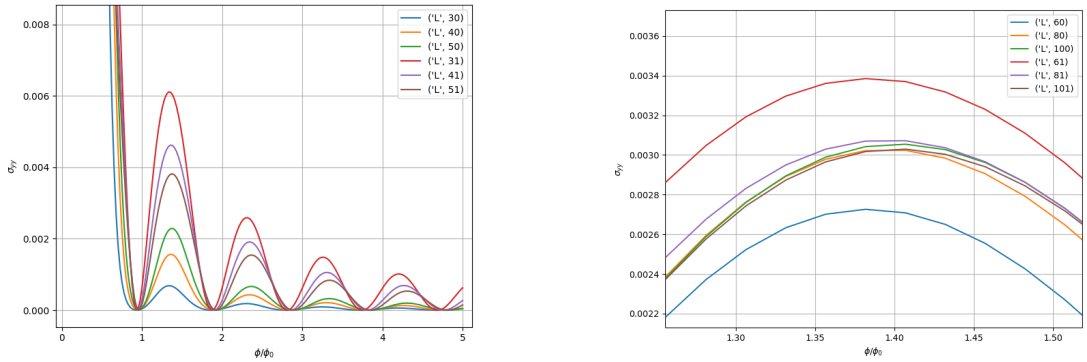

Figure 34: Intra-band conductivity at different width. Here it was chosen EF=0. The left plot is zoomed to the first maximum.

The case of an isotropic system and a system containing small anisotropy, at increased number of channels $L = 300$, is shown in Fig.35. Also in the isotropic case the smooth periodic behaviour, observed at high anisotropy, crystallize out at higher channel number. This is in agreement with our model, where the periodicity comes from the magnetic flux and should be independent of the anisotropy.

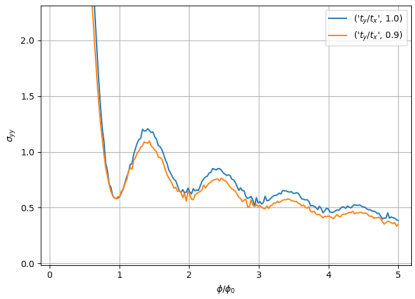

Figure 35: Intra-band conductivity as a function of magnetic flux at a temperature $k_BT = 0.02$. The calculation was done for an isotropic system and the case of small anisotropy, for a channel number of $L = 300$.

Inter-band conductivity

Fig.36 shows the inter-band conductivity as function of total flux. The behaviour differs from the intra-band one. However, after the first maximum, it decreases for increasing flux similar to the intra-band contribution. Consider the approximation of the group velocity eq.(103). Its behaviour is shown in Fig.37. Because the intra-band case was roughly proportional to the square of this function, a steep increase when going to smaller fluxes was observed. The behaviour of the non-squared group velocity can be adapted for the inter-band case. This is the case, because also there calculating the expectation values of the velocity operator between two bands, the flux dependence is induced by a sinus. The decrease at higher flux can be explained the same way, by the denominator of the group velocity. The question remains, why for integer flux values the conductivity is not zero. But this is just based on the fact, that even for flat bands, the inter-band hopping probability is not zero such that a finite conductivity remains. The increase of conductivity with higher temperature observed in subfigure **c)** is again an effect of dealing with small channel number L. However, this reveals the effect of anisotropy in systems that contain a large level spacing. Both together favours the separation of the levels. This has the effect that the thermal energy scale k_BT, at small temperatures, reaches only a few levels. The higher values given by the Fermi distribution, compared to the high temperature case, are not able to overcome this difference, resulting in the observed behaviour. Subfigure **d)** shows a non-converging increase of the conductivity with increasing L. It turns out, that the increase goes nearly linear with the sample width. This leads us to the main scaling problem also the authors in [5] were confronted with.

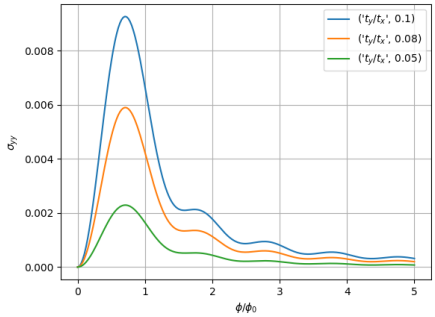

(a) $k_BT = 0.02$

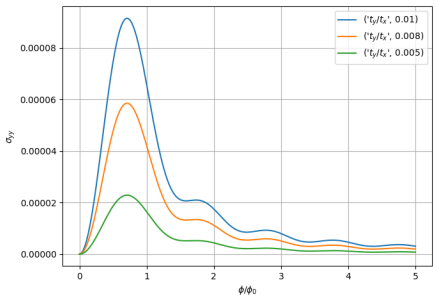

(b) $k_BT = 0.02$

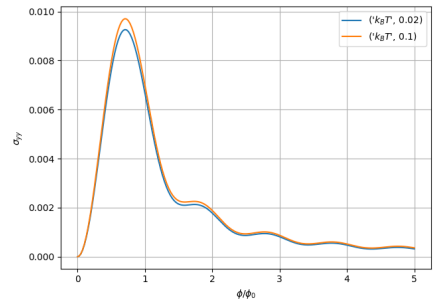

(c) $\kappa = 0.1$

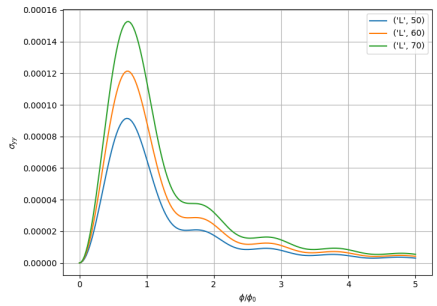

(d) $\kappa = 0.1$, $k_BT = 0.02$

Figure 36: Inter-band conductivity as a function of total flux. **a,b)**: shows the effect of anisotropy at fixed temperature; **c)**: behaviour under different temperatures at fixed anisotropy; **d)**: plotted for different width, at fixed temperature and anisotropy.

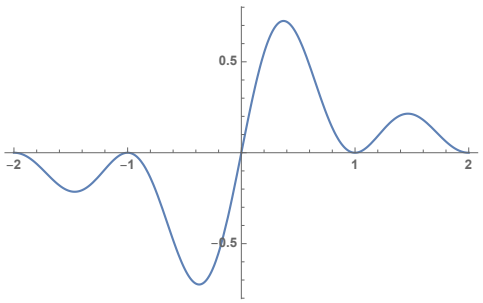

Figure 37: Total amplitude $\mathrm{Im}\, A(x)$ plotted form -2 to 2, to show the general behaviour.

Combined conductivity

To get the total Kubo conductivity one has to take the sum of both contributions inter- and intra-band. We will study the whole conductivity and resistivity in the case of strong anisotropy, to be able to compare the results with the experimentally observed behaviour in [5]. To do this, one has to take the values of η in a range calculated in

section 5.3. But then one would has to deal with the real width of $L \approx 8000$, what is because of available computational power impossible. For the chosen Fermi energy and for η in that range, the inter-band conductivity scales nearly linear with L. Thus we can express the scaling of a system of size $L = 8000$, to one of size $L = 50$, by scaling the parameter η, such that it is placed in a range of approximately 0.03 to 0.07. This again leads to another problem with the intra-band contributions. Because they would be, for the real values of η, huge compared to the inter-band contributions and clearly dominate the full conductivity. To have comparable contributions we took also for the intra-band conductivity the rescaled parameter.

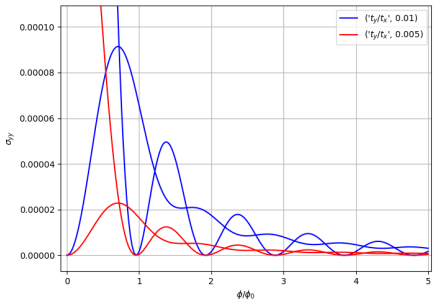

(a) $\eta = 0.05$

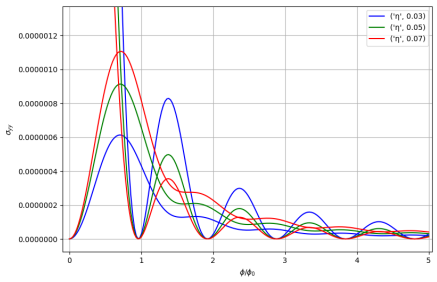

(b) $\kappa = 0.001$

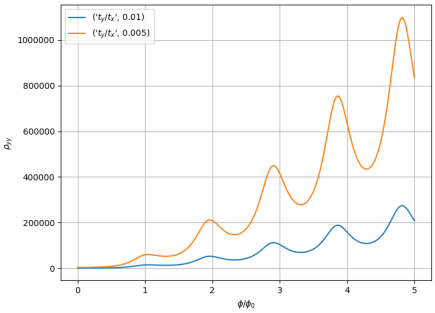

(c) $\eta = 0.05$.

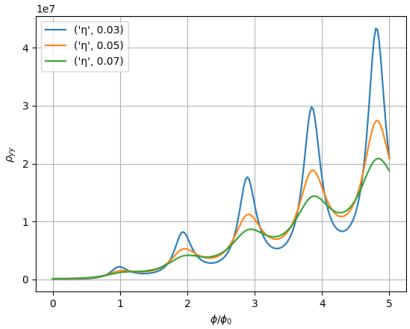

(d) $\kappa = 0.001$

Figure 38: **a,b)**:compined conductivity as a function of magnetic flux. Subfigure **a)** shows the effect of different anisotropy, for fixed η; **b)** shows the effect of changing η for a fixed anisotropy κ. **c,d)**: resistivity calculated form the inverse of the sum of both contributions, for the cases in **a,b)**

Fig.38 shows both contributions compared to each other in subfigure **a,b)** and the resistivity calculated from the inverse sum of both contributions in subfigure **c,d)**. One observes, that a decrease in anisotropy increases the gap between the maximum of the intra-band conductivity and minima of inter-band conductivity. This steeper increase of the intra-band contribution against the inter-band one shows again that the inter-band

conductivity is not simple linked to the band-curvature, as it is the case for the intra-band conductivity. The inter-band contribution lifts the minima of the intra-band contribution, such that the resistivity do not diverge at integer flux values. Then the resistance shows also an oscillatory behaviour, with an oscillation period equal to the one determined by ϕ_0 threading the area S. Note: also here, in the limit of large L, the peaks will be exactly placed at integer flux values. This behaviour is similar to the one observed in the experiment, see Fig.39. However, at this state we are not able to get the experimentally observed behaviour without introducing a factor r with which we reduce the intra-band conductivity. Such a factor was also used in [5], $r_{we} = 0.0065$, $r_{paper} = 0.0075$. The benefit in our approach is that we have used the right temperature and anisotropy related to the experiment and used the same parameter η, resulting from included scattering contributions.
Without this factor only the intra-band contribution is observable, similar to the case using Landauer formalism. Thus the resistivity is expected to diverge.

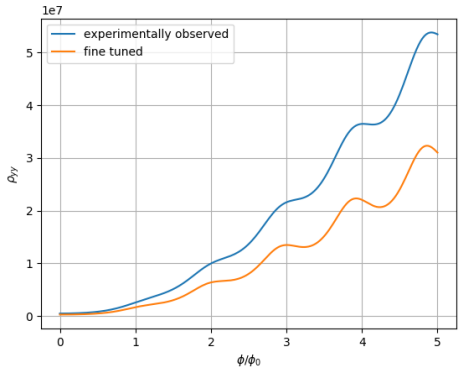

Figure 39: Comparison of the resistivity results observed in the experiment Fig.5C in [5] and the closest result we got, due to fine tuning of our model, in the given parameter range of η and κ in a range of 0.001 ± 0.0001.

Comparison Landauer and Kubo approach

We have seen that calculating the conductivity using the Landauer formula, leads most of the time to similar results as taking the intra-band Kubo formula. Comparing the magnitudes is difficult because of the open parameter η that is in this sense not included in the Landauer approach. Including disorder in the Landauer approach has the same effect as increasing η, such that it is lowering the conductivity. However, due to the way disorder was added, the reduction in conductivity turns out to be not linear to the disorder strength. In both cases, adding a random on-site potential or including hopping disorder, there is a huge decrease if the values reaches the one of the hopping amplitude. This reveals one of the main differences. Working with the Kubo formalism the non-equilibrium is reached due to an external electric field. Then the computation of non-equilibrium expectation values of physical operators, like the current density, is possible. The static (DC) conductivity is then given by the limit $\omega \to 0$ of the dynamic

conductivity. But even in this case, an electron has not to travel from one end of the sample to the other, it is enough if in total runs a current. In the Landauer theory the non-equilibrium is induced by the leads connecting the sample to the reservoirs. They contain a difference in particle-(charge) density, thus creating a potential difference (V_{bias}). Because the transport is then treated as a scattering problem the particle has to move from one end to the other. Thus if the disorder potential is of the order of the hopping amplitude, the particle is not reaching the other end and no current can flow.

The periodic behaviour in magnetic field with a period of one flux quantum is in both cases coming from the velocity operator. This can be seen for example in eq.(116). It shows that also in the case of the Landauer formalism, the expectation value of the velocity operator for each band separately is included. Thus if the band has zero bandwidth, like at the integer flux values, also Landauer conductivity turns to zero.

The effect of inter-band contribution was not observed in the Landauer approach. We can at this state not be absolutely sure that it would not be observable in the limit of large L, with included disorder. But we expect, because of the arguments given above, that at integer flux values it will always turn to zero.

8.3. Transversal conductivity

Fig.40 shows the result for the transversal conductivity, calculated with eq.(99) derived by the Kubo approach.

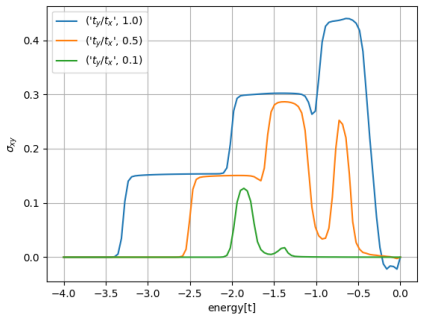

(a) $\Phi = \pi/4$

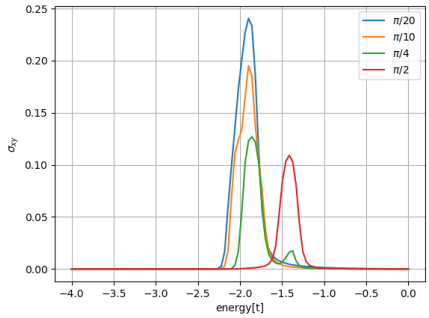

(b) $\kappa = 0.1$

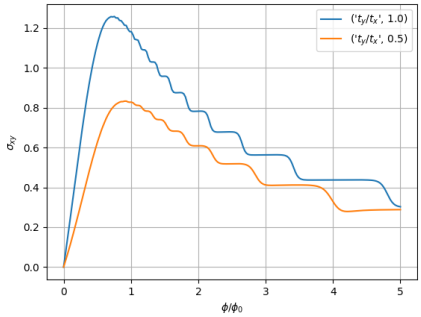

(c) $E_F = -1.5$.

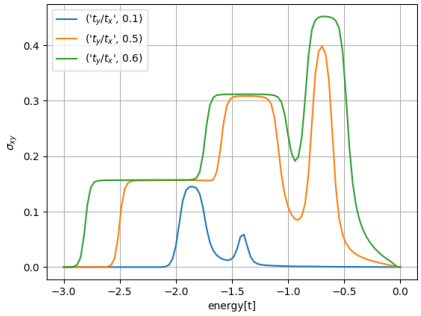

(d) $\Phi = \pi/4$

Figure 40: Transversal conductivity calculated at $\eta = 0.05$ and a temperature of $k_B T = 0.02$. Subfigure **a)** shows the vanishing of the conductivity plateaus with increasing anisotropy and fixed flux per plaquette; **b)** conductivity at fixed anisotropy and increasing flux per plaquette Φ; **c)** step wise decrease of the conductivity with increasing flux, at different anisotropy. A Fermi energy of $E_F = -1.5$ was chosen; **d)** conductivity at different anisotropy and fixed flux per plaquette, for an increased number of channels $L = 200$.

In the case of isotropic hopping one observes the contribution from the q-bands, in a way that characteristic Hall plateaus where build. Note: at an energy $E_F = 0$ we observe a strange behaviour. This is, because at that energy the bulk Dirac points are situated in the spectrum. The strong degeneracy should be handled numerically special, which was not done in this case because we are dealing in the following with an energy of $E_F = -1.5$. It is just to note, that this behaviour has no physical meaning. With increasing anisotropy the plateaus vanishes and just a single peak at the outer energy regions remains. Subfigure **b)** reveals a flux dependency of the peak position. The

position is in agreement with the position of the remaining edge states Fig.41. In section 3.2 it was observed that the inner bands hybridize to one band of very low density and with no observable edge states. Note: with further increase of the anisotropy all edge states gapped out and the peaks are placed at the outer bands, where maximal DOS is located.

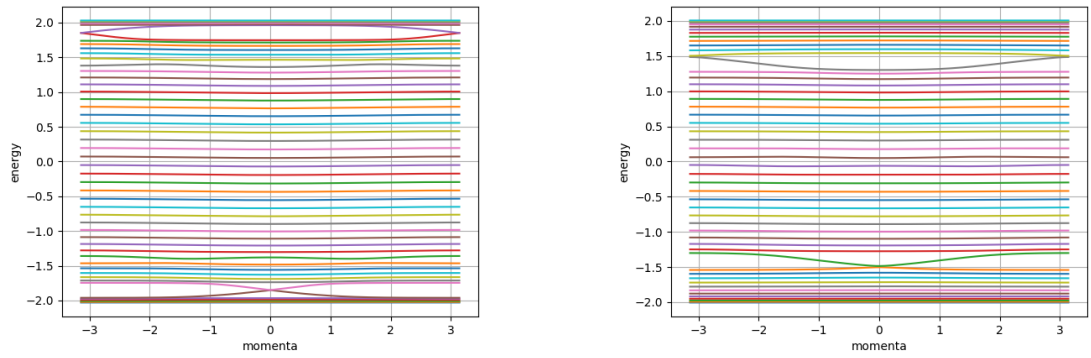

Figure 41: Energy spectrum for a system of size $L = 50$ at fixed anisotropy $\kappa = 0.1$. **Left**: $\Phi = \pi/4$; **Right**: $\Phi = \pi/2$.

The vanishing of the well separated bands does not automatically imply the break down of the Hall conductivity. Here we refer to [29]. There the authors described a similar case of vanishing bands for irrational flux values. They showed that also in the case of non well defined bands, the Hall physics is fully described by the number of edge states and as long as they remain the conductivity is well defined. If the anisotropy is not to strong, the plateaus seems to slightly come back with increasing channel number, see subfigure **d)**. This is what we expected from the results of section 3.2, where the gap was getting closed and the edge states remains. However for the case of an anisotropy of $\kappa \leq 0.1$, no such tendency was observed.

This implies that the edge states, for increasing level number L, do not remain if the anisotropy is to large. That is rather surprising due to the fact that the inversions symmetry of the spectrum, which is protecting the edge states, seems still to hold. At this state we make the following assumption. Working with finite dimension in x-direction, thus do not assume periodic boundary conditions, leads in the BZ to a topology that is different from the one of a torus. But studying Hall conductivity needs, as far as we know, exactly this underlying topology. Thus quantities as TKKN-invariants are not well defined without it. Therefore the considered protection of the edge states, due to symmetry, is not available.

9. Conclusion

We studied the effect of anisotropy on a two dimensional lattice, placed in an homogeneous magnetic field, given by an anisotropic Hofstadter model. The system has the special geometry of its width being smaller than the mean free path and is infinite in y direction. Thus working in a ballistic transport regime in x-direction.

A competition between the effect of the magnetic field and the anisotropy was observed. In the isotropic case the magnetic field turns the spectrum in to the well known Hofstadter butterfly structure and clustering the levels in to q bands. This effect is an interplay of lattice potential and magnetic field. Increasing anisotropy reduces the effect of the magnetic field, what leads to a domination of the lattice. Due to this, the spectrum turns in to L energetically separated levels, where L corresponds to the lattice width, thus to the number of transversal modes in the case of attached leads. These levels reveal a periodic broadening due to the magnetic field. Such a periodic behaviour is also reflected in the longitudinal conductivity. The role of anisotropy depends strongly on the level spacing, entering as an effect of the finite lattice width. Increasing anisotropy reduces the bandwidth because of a decreasing band curvature. This enhances the energetically separation of the levels. This level separation has a strong effect on the DOS. Whereas it is usually maximal at the position of the q bands, due to the separation it turns in an oscillatory behaviour with maxima at the level position and dominating peaks at the energy edges. The conductivity as a function of energy follows the DOS, with equally placed peaks. Consider the conductivity as a function of magnetic flux reveals a strong dependence in its oscillatory behaviour on the strength of the anisotropy. There, smooth oscillations could be only observed in the limit of large anisotropy. With increasing number of levels, thus increasing width, a well defined oscillatory behaviour could be also observed for the isotropic case. This shows that in the case of large L, the effect of anisotropy on the longitudinal conductivity, as a function of magnetic flux, is just a scaling effect.

When studying the band structure, a hybridization of the inner energy bands and thus vanishing of the edge states, as an effect of the anisotropy was observed. This has a huge impact on the transversal conductivity. Due to the missing of the underlying topology of a torus, there is no protection of the edge states due to the spectrum related symmetry. Thus even in the case of large L, the states gapped out under the effect of anisotropy and the Hall plateaus vanishes. This reveals again the domination oft the anisotropy over the effect of the magnetic field, when the conductivity is turned from showing Hall plateaus to a simple peak at the maximal DOS.

The longitudinal conductivity was calculated in the framework of Landauer Buettiker and Kubo. We could show a similar result between the intra-band Kubo conductivity and the conductivity calculated in the Landauer formalism. We could not observe a behaviour similar to the inter-band one, when working in the Landauer formalism. This does however not contradict the shown equivalence in chapter 6. There periodic boundary

conditions in x-direction were assumed. Our calculations, using the parameters from the experiment [5], has shown that the longitudinal conductivity is remarkably dominated by the intra-band contribution. Thus without introducing an additional scaling factor, that reduces the intra-band contribution, no inter-band conductivity would be visible. This in some case reveals the benefit of the Kubo approach, because of the possibility to treat intra- and inter-band contributions differently.

Appendices

A. Aharonov-Bohm approach

Here we try to give an understanding of why an Aharonov-Bohm like approach fails to explain the new observed oscillation of the magnetoresistance in [5]. Therefore we will give first an general introduction.

Aharonov-Bohm effect in metal rings

For a given vector potential, the electronic wave function is given by

$$\psi(\vec{r}) = \psi_0(\vec{r}) \exp\left(-\frac{ie}{\hbar c}\int \vec{A}\cdot d\vec{r}\right), \tag{126}$$

where ψ_0 is the wave function related to the case $\vec{A} = 0$. One can see that even if there is no physical field $\vec{B}$ in the path the electron passed, the vector potential has an effect on the electronic behaviour. This is the Aharonov-Bohm effect (ABE) and independent of the sample geometry [2].
Consider a ring, where flux is pierced through its center. For this geometry there are two possible ways γ_1,γ_2 the electron can move. This leads to the following wave functions

$$\psi_1(\vec{r}) = \psi_0 \exp\left(\frac{ie}{\hbar c}\int\limits_{\gamma_1} \vec{A}\cdot d\vec{r}\right) \tag{127}$$

$$\psi_2(\vec{r}) = \psi_0 \exp\left(\frac{ie}{\hbar c}\int\limits_{\gamma_2} \vec{A}\cdot d\vec{r}\right). \tag{128}$$

The electron density on the screen is given by

$$|\psi_1 + \psi_2|^2 = 2|\psi_0|^2 + 2|\psi_0|^2 \cos\left(\frac{2\pi\Phi}{\phi_0}\right), \tag{129}$$

with

$$\Phi = \int\limits_{\gamma_1-\gamma_2} \vec{A}\cdot d\vec{r} = \oint \vec{A}\cdot d\vec{l} = \int\limits_{\partial V} \vec{B}\cdot d\vec{S} \tag{130}$$

the magnetic flux enclosed by the paths and $\phi_0 = hc/e$ the magnetic flux quantum for a system of single-electrons.
When the flux increases, the interference fringes will move periodically, with a period of a magnetic flux quantum.

Altshuler-Aronov-Spivak effect

Consider the oscillation of the magnetoresistsance as a function of the magnetic field. Beside a peak that represents the ABE oscillation, there is another peak, thus another

oscillation (much weaker) with period corresponding to magnetic flux of $hc/2e$. This oscillation comes from the Altshuler-Aronov-Spivak effect (AASE) [32]. Consider a magnetic flux Φ enclosed by a loop. Then the change of the phase, of the electronic wave function, depends on the direction the path goes around the loop. Let $-\Delta\phi_1$ be for positive direction and $\Delta\phi_2$ for negative direction. When the paths goes twice around the loop, the electron wave function meets at the same point and $\Delta\phi_1 - \Delta\phi_2 = 2\Phi$, which leads to an interference effect with period $hc/2e$

$$\psi_1^*\psi_2 + \psi_1\psi_2^* = 2|\psi_0|^2 \cos\left(\frac{4\pi\Phi}{\phi_0}\right). \tag{131}$$

For this effect to occure, weak disorder is needed. Scattering on the impurites enhances backscattering which leads to interference of electron waves and therefore to weak localization. Without it, the probability for the path to goes around the loop twice and therefore the AASE, is vanishing.

Reason of failure

In the case of our system applying an Aharonov-Bohm approach, the quasiparticle would encircle the area S, where the conducting layers behaves like the arms of the interferometer. Beside the fact that ABE in metallic rings was only observed for temperatures below $1K$ and the authors in [5] observed oscillations up to $60K$, there are two main reasons of failure.

-) Starting at one edge the quasiparticle would have to travel along the conducting lead to the other edge, without hopping between the layers. But due to the coupling t_y, that is too strong for such a condition, it would tunnel many times between the layers, resulting in destructive interference.

-) If the ABE approach would be correct, one would also have to see an oscillation with half period $h/2e$ because of the AASE. Such a peak in frequency was not observed but it could be that it still exists, covered by the noise. However, the needed weak localization due to enhanced backscattering, would lead to an increasing hopping probability and therefore raising the chance of destructive interference.

B. Kubo-Bastin formula

Here we show, that our derived formula for the Kubo conductivity eq.(91), can be written in a representation free way leading to the Kubo-Bastin formula for DC conductivity. Use

$$\lim_{\eta\to 0^+}\frac{1}{(\varepsilon_n-\varepsilon)(\varepsilon_n-\varepsilon+i\eta)}=\lim_{\eta\to 0^+}\frac{d}{d\epsilon}\left(\frac{1}{\varepsilon_n-\varepsilon+i\eta}\right) \tag{132}$$

and $\int_{-\infty}^{\infty}d\varepsilon(\varepsilon-H_0)=1$ to write eq.(91) as

$$\begin{aligned}\sigma_{yy}^{DC}=&\frac{i}{L}\int_{-\infty}^{\infty}d\varepsilon f(\varepsilon)\sum_{n,m}^{L}\int_{-\pi}^{\pi}\frac{dk_y}{2\pi}\left(\langle n|\hat{j}_y|m\rangle\frac{d}{d\varepsilon}\left(\frac{1}{\varepsilon-\varepsilon_m+i\eta}\right)\langle m|\hat{j}_y|n\rangle\delta(\varepsilon-\varepsilon_n)\right.\\&\left.-\langle m|\hat{j}_y|n\rangle\delta(\varepsilon-\varepsilon_m)\langle n|\hat{j}_y|m\rangle\frac{d}{d\varepsilon}\left(\frac{1}{\varepsilon-\varepsilon_n+i\eta}\right)\right).\end{aligned} \tag{133}$$

Introducing the retarded and advanced Green function $G^{\pm}(\varepsilon)=\frac{1}{\varepsilon-\hat{H}_0\pm i\eta}$ and rewrite the above equation in operator form

$$\sigma_{yy}^{DC}=\frac{i}{L}\int_{-\infty}^{\infty}d\varepsilon f(\varepsilon)Tr\left\{\int_{-\pi}^{\pi}\frac{dk_y}{2\pi}\left(\hat{j}_y\frac{dG^+(\varepsilon)}{d\varepsilon}\hat{j}_y\delta(\varepsilon-\hat{H}_0)-\hat{j}_y\delta(\varepsilon-\hat{H}_0)\hat{j}_y\frac{dG^-(\varepsilon)}{d\varepsilon}\right)\right\} \tag{134}$$

Note that the k-integration has to be done component wise.
The δ-functions makes this formula very demanding to treat it numerically. A way out of this is two rewrite the δ-functions in terms of Green functions

$$\delta(\varepsilon-\hat{H}_0)=-\frac{1}{2\pi i}\left[G^+-G^-\right]. \tag{135}$$

Rewriting eq.(134) using (135) one gets

$$\boxed{\begin{aligned}\sigma_{yy}^{DC}=&-\frac{1}{L}\int_{-\infty}^{\infty}d\varepsilon f(\varepsilon)Tr\left\{\int_{-\pi}^{\pi}\frac{dk_y}{(2\pi)^2}\left(\hat{j}_y\frac{dG^+(\varepsilon)}{d\varepsilon}\hat{j}_y\left[G^+-G^-\right]\right.\right.\\&\left.\left.-\hat{j}_y\left[G^+-G^-\right]\hat{j}_y\frac{dG^-(\varepsilon)}{d\varepsilon}\right)\right\}\end{aligned}} \tag{136}$$

This is the Kubo-Bastian formula for the DC-conductivity. It seems that eq.(136) depend on the whole set of occupied states. But Streda (1982) [33] has proven that the conductivity only depends on the properties of the system around the Fermi level. This legitimate us to just do integration by parts and neglect the boundary terms.

$$\begin{aligned}\sigma_{yy}^{DC}=&\frac{1}{L}\int_{-\infty}^{\infty}d\varepsilon\frac{\partial f(\varepsilon)}{\partial\varepsilon}Tr\left\{\int_{-\pi}^{\pi}\frac{dk_y}{(2\pi)^2}\left(\hat{j}_yG^+(\varepsilon)\hat{j}_y\left[G^+-G^-\right]\right.\right.\\&\left.\left.-\hat{j}_y\left[G^+-G^-\right]\hat{j}_yG^-(\varepsilon)\right)\right\}\end{aligned} \tag{137}$$

C. Phase factor

Calculation of the phase factor eq.(123). In the following calculations we have chosen Landau gauge $\vec{A} = (0, Bx, 0)^T$. Fig.42 shows a schematic picture of one lattice unit cell, with the curve moving counter clockwise around it, used to calculate the magnetic flux.

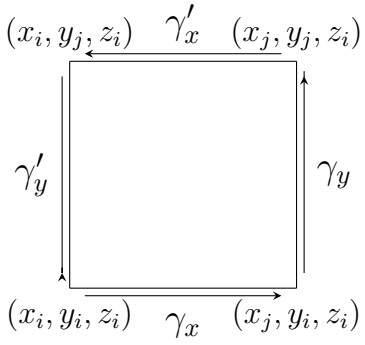

Figure 42: Schmatic drawing of the lattice unit cell, with the curve used to calculate the enclosed magnetic flux

The path integral defining the magnetic flux, which pierces the unit cell, is given by

$$\int_\gamma \vec{A} d\vec{s} = \int_a^b \vec{A}(\gamma(t)) \cdot \dot{\vec{\gamma}}(t) dt, \tag{138}$$

where the curve is defined as an image $\gamma : [a, b] \to \mathbb{R}^3$. For a rectangle the parameters are $a = 0, b = 1$. We calculated the contribution of the paths γ_x, γ_y and γ'_y explicitly. The ones from γ'_x can be calculated the same way, leading to an equivalent result.

$$\vec{\gamma}_x = (x_i + t(x_j - x_i), y_i, z_i)^T, \qquad \dot{\vec{\gamma}}_x = ((x_j - x_i), 0, 0)^T \tag{139}$$

$$\int_0^1 \vec{A}(\gamma_x(t)) \cdot \dot{\vec{\gamma}}_x(t) dt = \int_0^1 \begin{pmatrix} 0 \\ B(x_i + t(x_j - x_i)) \\ 0 \end{pmatrix} \cdot \begin{pmatrix} (x_j - x_i) \\ 0 \\ 0 \end{pmatrix} dt = 0 \tag{140}$$

$$\vec{\gamma}_y = (x_j, y_i + t(y_j - y_i), z_i)^T, \qquad \dot{\vec{\gamma}}_x = (0, y_j - y_i, 0)^T \tag{141}$$

$$\int_0^1 \vec{A}(\gamma_y(t)) \cdot \dot{\vec{\gamma}}_y(t) dt = \int_0^1 \begin{pmatrix} 0 \\ Bx_j \\ 0 \end{pmatrix} \cdot \begin{pmatrix} (y_j - y_i) \\ 0 \\ 0 \end{pmatrix} dt = Bx_j(y_j - y_i) \tag{142}$$

$$\vec{\gamma'}_y = (x_i, y_j + t(y_i - y_j), z_i)^T, \qquad \dot{\vec{\gamma}}'_x = (0, y_i - y_j, 0)^T \tag{143}$$

$$\int_0^1 \vec{A}(\gamma'_y(t)) \cdot \dot{\vec{\gamma}}'_y(t) dt = \int_0^1 \begin{pmatrix} 0 \\ Bx_i \\ 0 \end{pmatrix} \cdot \begin{pmatrix} (y_i - y_i) \\ 0 \\ 0 \end{pmatrix} dt = Bx_i(y_i - y_j) \tag{144}$$

Taking the average and note that $\phi \overset{a=1}{\overbrace{=}} B$ leads to the phase factor in eq.(123).

D. S-matrix in Kwant

To understand how Kwant calculate the scattering matrix, following the documentation of TC.Gorth [22], we focus on the wave function formulation of the scattering matrix problem due to its simpler structure compared to a formulation with non-equilibrium Green's functions.

Several leads can always be considered as one effective lead with disjoint section, therefore we can focus on just one single lead. Choosing a basis in which the sites are ordered according to the distance to the scattering region, in a reverse order. Means the Hamiltonian has a tridiagonal block form, last the scattering region S, then the unit cells starting from the first one attached to S.

$$H = \begin{pmatrix} \ddots & V_L & & \\ V_L^\dagger & H_L & V_L & \\ & V_L^\dagger & H_L & V_{LS} \\ & & V_{LS}^\dagger & H_S \end{pmatrix}, \tag{145}$$

where H_S is the Hamiltonian matrix of the scattering region and H_L the one of one unit cell of the lead. V_L and V_{LS} are the block submatrix Hamiltonians connecting different unit cells in the lead and defining the hopping between the lead and the scattering region. For the system we define the wave function Ψ^S of the scattering region and $\Psi^L(i)$ the one for the i-th unit cell. Due to the translational invariance of the leads, the wave functions can be written as a superposition of plane waves. The eigenstates of the translation operator in the lead take the form

$$\psi_n(j) = \lambda_n^j \vartheta_n \tag{146}$$

obeying the Schroedinger equation in the lead

$$\left(H_L + V_L\lambda_n^{-1} + V_L^\dagger \lambda_n\right)\vartheta_n = E\vartheta_n, \tag{147}$$

with ϑ_n, λ_n the n-th eigenvector, eigenvalue. Due to the normalizability of the wave function $|\lambda_n| \leq 1$, there are evanescent modes $|\lambda_n| < 1$ and propagating ones $\lambda_n = e^{ik_n}$, with k_n the longitudinal momentum of mode (channel) n. Note: the description in terms of k_n is only possible because we are dealing with an infinite system in longitudinal direction. The propagating modes are normalized according to the expectation value of the particle current

$$\langle I \rangle = 2Im\langle \psi_n(j)|V_L|\psi_n(j-1)\rangle = \pm 1. \tag{148}$$

By sorting the modes into incoming $\psi_n^{in}(\langle I\rangle = +1)$, outgoing $\psi_n^{out}(\langle I\rangle = -1)$ and evanescent ones $\psi_n^{ev}(\langle I\rangle = 0)$, the scattering states in the leads take the form

$$\Psi_n(i) = \psi_n^{in}(i) + \sum_m S_{mn}\psi_m^{out}(i) + \sum_p \tilde{S}_{pn}\psi_p^{ev}(i) \tag{149}$$

and the scattering wave function inside the system is given by

$$\Psi_n(0) = \psi_n^S. \tag{150}$$

Kwant calculates S_{nm} and ψ_n^S in a way, that it matching the wave function in the leads with the one in the scattering region. This amounts to inserting the above form of the wave function into the thight-binding equations $H\Psi_n = \varepsilon\Psi_n$, with H given by eq.(145).

References

[1] C.J.Davisson and L.H. Germer:
Reflection of Electrons by a Crystal of Nickel.
Proc. Natl. Acad.Sci. United States Am. 14, 317-322 (1928)

[2] V.Chandrasekhar, M.J.Rooks, S.Wind and D.E.Prober
Observation of Aharonov-Bohm electron interference effects with periods he and h2e in individual micron-size, normal-metal rings.
Phys. Rev. Lett. 55, 1610-1613 (1985)

[3] C.W.Hicks et al.
Quantum oscillations and high carrier mobility in the delafossite PdCoO2.
Phys. Rev. Lett. 109, 1-5 (2012)

[4] D.Shoenberg
Magnetic oscillations in metals.
(Cambridge University Press, 1984): doi:10.1017/CBO9780511897870

[5] C. Putzke, M.D.Bachmann et all.:
h/e Oscillations in Interlayer Transport of Delafossites. (2019) , arXiv:1902.07331

[6] Feng Duan and Jin Guojun, Book:
Introduction to Condensed Matter Physics, Volume 1, chapter 10.1

[7] Carlo Jacoboni, Book:
Theory of Electron Transport in Semiconductors, chapter 18.2

[8] Feng Duan and Jin Guojun, Book:
Introduction to Condensed Matter Physics, Volume 1, chapter 9.2

[9] Gerd Czycholl, Book:
Theoretische Festkoerperphysik, Band 2, Chapter 1.10

[10] Aidelsburg, M., Book:
Artificial Gauge Fields with Ultracold Atoms in Optical Lattices. 2016, XIII, Chapter 2

[11] A. Messiah:
Quantum Mechanics (Wiley, New York, 1965), Vol, II, Chap. 19.

[12] Douglas R. Hofstadter:
Energy levels and wave functions of Bloch electrons in rational and irrational magnetic fields
Physical Review B, Volume 14, Number 6, Sept, 1976

[13] David Tong:
The Quantum Hall Effect; TIFR Infosys Lectures; Chap. 2.3.3
arXiv:1606.06687v2 [hep-th] 20 Sep 2016

[14] David Tong:
The Quantum Hall Effect; TIFR Infosys Lectures; Chap. 2.3.3, page 70/71
arXiv:1606.06687v2 [hep-th] 20 Sep 2016

[15] K.Chadova:
Electronic Transport Within the Kubo-Bastin Formalism
PhD Thesis: https://nbn-resolving.org/urn:nbn:de:bvb:19-216095

[16] Monika Aidelsburger, Book:
Artificial Gauge Fields with Ultracold Atoms in Optical Lattices.
2016, Chapter 2.3.2

[17] Shuichi Murakami
Two-dimensional topological insulators and their edge states.
2011 J. Phys.: Conf. Ser. 302 012019

[18] Michael V. Moskalets, Book:
Scattering Matrix Approach to Non-Stationary Quantum Transport.
Chapter 1: Landauer Buettiker formalism

[19] Michael E.Peskin, Book:
An Introduction to Quantum Field Theory.
Chapter 3.5

[20] Tibor Sekera:
Quantum transport of fermions in honeycomb lattices and cold atomic systems.
Phd Thesis at University of Basel: http://edoc.unibas.ch/diss/DissB_12848
Chapter 2.7

[21] TC.W. Groth, M.Wimmer et al.
Kwant 1.4.0 documentation.
Official Kwant documentation: *https://downloads.kwant−project.org/doc/latest.pdf*

[22] TC.W. Groth, M.Wimmer et al.
Kwant: a software package for quantum transport.
arXiv:1309.2926v1 [cond−mat.mes−hall] 11 Sep 2013

[23] R. Kubo
Statistical-mechanical theory of irreversible processes. I. General theory and simple applications to magnetic and conduction problems.
J. Phys. Soc. Japan 12, 564 (1957)

[24] Laszlo Szunyogh
Theory of Electric Transport, chapter 2.3.
2009, Department of Theoretical Physics Budapest University of Technology and Economics

[25] Czycholl, G. and Kramer, B.
Nonvanishing zero temperature static conductivity in one dimensional disordered systems..
Solid State Commun. 32, 945-951 (1979)

[26] J. Hajdu, M. Janflen, and O. Viehweger
Kubo Hall Conductivity on a Finite Cylinder and the Integer Quantum Hall Effect.
Z.Phys.B- Condensed Matter66,433-439(1987)

[27] F. Ortmann et. al.
Efficient Linear Scaling Approach for Computing the Kubo Hall Conductivity.
arXiv:1501.05100v1 [cond-mat.mes-hall] 21 Jan 2015

[28] B.K. Nikolic
Which Kubo formula gives the exact conductance of a mesoscopic disordered system.
arXiv:cond-mat/0103150v4 [cond-mat.mes-hall] 25 Oct 2001

[29] Igor N. Karnaukhov
Edge modes in the Hofstadter model of interacting electrons.
arXiv:1801.01425v2 [cond-mat.str-el] 30 Jan 2019

[30] P.Dutta, S.K.Maiti and S.N.Karmakar
Integer Quantum Hall Effect in a Lattice Model Revisited: Kubo Formalism.
arXiv:1202.1960v2 [cond-mat.mes-hall] 5 Mar 2012

[31] P.S.Fisher and P.A.Lee
Relation between conductivity and transmission matrix.
Physical Review B, Volume 23, Number 12, 1981

[32] B.L.Al'tshuler, A.G.Aronov and B.Z.Spivak
The Aaronov-Bohm effect in disordered conductors.
Pis'ma Zh.Eksp.Teor.Fiz.33,No.2,101-103 (20 January 1981)

[33] P.Streda
Theory of quantised Hall conductivity in two dimensions.
J. Phys. C: Solid State Phys. 15, L717 (1982).